Two-parameter scaling theory of the longitudinal magnetoconductivity in a Weyl metal phase: Chiral anomaly, weak disorder, and finite temperature

Kyoung-Min Kim,[1] Dongwoo Shin,[1] M. Sasaki,[2] Heon-Jung Kim,[3] Jeehoon Kim,[1,4] and Ki-Seok Kim[1]
[1]*Department of Physics, POSTECH, Pohang, Gyeongbuk 790-784, Korea*
[2]*Department of Physics, Faculty of Science, Yamagata University, Kojirakawa, Yamagata 990-8560, Japan*
[3]*Department of Physics, College of Natural Science, Daegu University, Gyeongbuk 712-714, Korea*
[4]*Center for Artificial Low Dimensional Electronic Systems, Institute for Basic Science, 77 Cheongam-Ro, Nam-Gu, Pohang 790-784, Korea*
(Received 23 May 2016; revised manuscript received 26 July 2016; published 15 August 2016)

It is at the heart of modern condensed matter physics to investigate the role of a topological structure in anomalous transport phenomena. In particular, chiral anomaly turns out to be the underlying mechanism for the negative longitudinal magnetoresistivity in a Weyl metal phase. The existence of a dissipationless current channel causes enhancement of electric currents along the direction of a pair of Weyl points or applied magnetic fields (B). However, temperature (T) dependence of the negative longitudinal magnetoresistivity has not been understood yet in the presence of disorder scattering since it is not clear at all how to introduce effects of disorder scattering into the topological-in-origin transport coefficient at finite temperatures. The calculation based on the Kubo formula of the current-current correlation function is simply not known for this anomalous transport coefficient. Combining the renormalization group analysis with the Boltzmann transport theory to encode the chiral anomaly, we reveal how disorder scattering renormalizes the distance between a pair of Weyl points and such a renormalization effect modifies the topological-in-origin transport coefficient at finite temperatures. As a result, we find breakdown of B/T scaling, given by $B/T^{1+\eta}$ with $0 < \eta < 1$. This breakdown may be regarded to be a fingerprint of the interplay between disorder scattering and topological structure in a Weyl metal phase.

DOI: 10.1103/PhysRevB.94.085128

I. INTRODUCTION

Researches on the role of topological-in-origin terms in quantum phases and their transitions have been a driving force for modern condensed matter physics, which cover quantum spin chains [1] and deconfined quantum criticality [2,3], quantum Hall effects and topological phases of matter [4], Anderson localization for the classification of topological phases and their phase transitions [5], and so on. In particular, renormalization effects of such topological terms are responsible for novel universality classes beyond the Landau-Ginzburg-Wilson paradigm of phase transitions with symmetry breaking. However, it is quite a nontrivial task to perform the renormalization group analysis in the presence of the topological-in-origin term, even if it can be taken into account perturbatively for the contribution of a bulk sometimes. Frequently, nonperturbative effects should be introduced into the renormalization group analysis [6,7], uncontrolled in this situation and thus, being under debate as an open question.

In this study we investigate disorder-driven renormalization of a topological-in-origin term referred to as an inhomogeneous θ term in three spatial dimensions [8], defined by

$$\mathcal{F} = -\frac{1}{\beta}\int_{-\infty}^{\infty} dv(\boldsymbol{r})P[v(\boldsymbol{r})]\ln\int D\bar{\psi}(\boldsymbol{r},\tau)D\psi(\boldsymbol{r},\tau) \times \exp\left\{-\int_0^\beta d\tau\int d^3\boldsymbol{r}\left[\bar{\psi}(\boldsymbol{r},\tau)i\gamma_\mu[\partial_\mu - ieA_\mu(\boldsymbol{r},\tau)] \times\psi(\boldsymbol{r},\tau) + v(\boldsymbol{r})\bar{\psi}(\boldsymbol{r},\tau)\gamma_\tau\psi(\boldsymbol{r},\tau) - \frac{1}{4}F_{\mu\nu}(\boldsymbol{r},\tau)F_{\mu\nu}(\boldsymbol{r},\tau) + \theta(\boldsymbol{r})\frac{e^2}{16\pi^2}\varepsilon_{\mu\nu\gamma\delta}F_{\mu\nu}(\boldsymbol{r},\tau)F_{\gamma\delta}(\boldsymbol{r},\tau)\right]\right\}. \quad (1)$$

$\psi(\boldsymbol{r},\tau)$ is a four-component Dirac spinor to describe an electron field of spin 1/2 in two orbitals. Its dynamics is given by a Dirac theory, where γ_μ with $\mu = (\tau,x,y,z)$ is a Dirac matrix to satisfy the Clifford algebra. $A_\mu(\boldsymbol{r},\tau)$ and $F_{\mu\nu}(\boldsymbol{r},\tau) = \partial_\mu A_\nu(\boldsymbol{r},\tau) - \partial_\nu A_\mu(\boldsymbol{r},\tau)$ are an externally applied electromagnetic field and its field strength tensor, respectively. $v(\boldsymbol{r})$ is a potential configuration, given randomly and described by the Gaussian probability distribution $P[v(\boldsymbol{r})] = \mathcal{N}\exp(-\int d^3\boldsymbol{r}\frac{[v(\boldsymbol{r})]^2}{2\Gamma})$. Γ is the variance of the disorder distribution and $\mathcal{N}$ is a normalization constant, determined by $\int_{-\infty}^{\infty} dv(\boldsymbol{r})P[v(\boldsymbol{r})] = 1$. The last term is an inhomogeneous θ term, topological in its origin and keeping chiral anomaly that the chiral current is not conserved in the quantum level [9], given by

$$\partial_\mu[\bar{\psi}(\boldsymbol{r},\tau)\gamma_\mu\gamma_5\psi(\boldsymbol{r},\tau)] = -\frac{e^2}{16\pi^2}\varepsilon_{\mu\nu\gamma\delta}F_{\mu\nu}(\boldsymbol{r},\tau)F_{\gamma\delta}(\boldsymbol{r},\tau). \quad (2)$$

γ_5 is a chiral Dirac matrix to anticommute with γ_μ. Here, the problem is how the inhomogeneous θ term becomes renormalized via the disorder scattering.

This problem can be cast into more physical terms. Introducing the chiral-anomaly equation into the effective field theory and performing the integration-by-parts for the chiral-current term with the $\theta(\boldsymbol{r})$ coefficient [10], we obtain

$$\mathcal{F} = -\frac{1}{\beta}\int_{-\infty}^{\infty} dv(\boldsymbol{r})P[v(\boldsymbol{r})]\ln\int D\bar{\psi}(\boldsymbol{r},\tau)D\psi(\boldsymbol{r},\tau) \times \exp\left\{-\int_0^\beta d\tau\int d^3\boldsymbol{r}\left[\bar{\psi}(\boldsymbol{r},\tau)i\gamma_\mu[\partial_\mu - ieA_\mu(\boldsymbol{r},\tau)]\right.\right.$$

 ©2016 American Physical Society

$$\times \psi(\boldsymbol{r},\tau) + c_\mu(\boldsymbol{r},\tau)\bar{\psi}(\boldsymbol{r},\tau)\gamma_\mu\gamma_5\psi(\boldsymbol{r},\tau) + v(\boldsymbol{r})\bar{\psi}(\boldsymbol{r},\tau)\gamma_\tau \times \psi(\boldsymbol{r},\tau) - \frac{1}{4}F_{\mu\nu}(\boldsymbol{r},\tau)F_{\mu\nu}(\boldsymbol{r},\tau)\Big]\Big\}. \quad (3)$$

$c_\mu(\boldsymbol{r},\tau) = \partial_\mu\theta(\boldsymbol{r})$ is referred to as chiral gauge field, regarded to be a background potential given by the inhomogeneous θ coefficient. When the background chiral gauge field serves a homogeneous potential, the resulting spectrum turns out to describe dynamics of Weyl electrons. The right-handed helicity part shifts into the right-hand side and the left-handed helicity part does into the left [11–13]. Physically, this homogeneous chiral-gauge-field potential is realized as $\boldsymbol{c} = \nabla\theta(\boldsymbol{r}) = g\boldsymbol{B}$, applying a homogeneous magnetic field $\boldsymbol{B}$ into a gapless semiconductor described above. The Dirac point separates into a pair of Weyl points along the direction of the applied magnetic field and the distance of the pair of Weyl points is proportional to the strength of the applied magnetic field with a Lande-g factor (see the Appendix). As a result, the previous mathematically defined problem is actually how the background chiral gauge field, more physically, the distance between a pair of Weyl points becomes renormalized by random elastic scattering.

The renormalization effect of the distance between a pair of Weyl points is measurable experimentally since the information is encoded into the negative longitudinal magnetoresistivity. This anomalous transport phenomena in a Weyl metal phase has been well known for more than thirty years [14] and experimentally confirmed in 2013 [15]. The electrical resistivity measured along the direction of the applied magnetic field becomes smaller than that measured in other directions. More quantitatively, the magnetoconductivity is enhanced in the longitudinal setup, i.e., $\boldsymbol{E}\|\boldsymbol{B}$, as follows:

$$\sigma_L(B) = \sigma_D(1 + \mathcal{C}_W B^2), \quad (4)$$

where $\boldsymbol{E}$ is an applied electric field [16]. σ_D is the Drude conductivity determined purely by disorder scattering. In real experiments, quantum corrections by weak antilocalization are introduced into the Drude conductivity [17]. $\mathcal{C}_W$ is a positive coefficient, discussed later in more detail. An essential point is that the enhancement of the longitudinal magnetoconductivity is given by the square of the distance between the pair of Weyl points. This longitudinal enhancement can be figured out in the following way: There exists a dissipationless current channel as a vacuum state, which connects the pair of Weyl points, responsible for the chiral anomaly. As a result, electrical currents are allowed to flow better along this direction through this vacuum channel although the measured longitudinal magnetoconductivity does not result from such dissipationless electrical currents [14]. When the distance between the pair of Weyl points is renormalized by random elastic scattering, the positive coefficient $\mathcal{C}_W$ would evolve as a function of an energy scale, here, temperature. It is natural to expect finding a scaling theory for the chiral-anomaly-driven enhanced longitudinal magnetoconductivity.

The above discussion reminds us of a two-parameter scaling theory for the Anderson localization in topological phases of matter [18], including the plateau-plateau transition in the integer quantum Hall effect [6]. There, the transport phenomenon of the Anderson localization transition is determined by the transverse conductivity σ_{xx} and the Hall conductivity σ_{xy}, where the latter encodes the topological information of the integer quantum Hall effect. The present situation is quite analogous to that of the integer quantum Hall effect. σ_{xx} in the quantum Hall effect is identified with the Drude conductivity σ_D, determined by disorder scattering directly. On the other hand, σ_{xy} in the quantum Hall effect is analogous to the distance between the pair of Weyl points, where the renormalization effect is introduced into the temperature dependence of $\mathcal{C}_W$. Recently, an effective nonlinear σ-model field theory has been derived for a Weyl metal phase, where several types of topological-in-origin terms are shown to appear [19].

In this study we investigate the longitudinal magnetoconductivity at finite temperatures and find a two-parameter scaling theory, where renormalization effects result from random elastic scattering. There is one difficult point in the calculation of the longitudinal magnetoconductivity in a Weyl metal phase. It turns out that a naive Kubo-formula calculation does not incorporate the role of the chiral anomaly in the longitudinal magnetoconductivity [20]. As a result, we fail to find the B^2 enhancement of the longitudinal magnetoconductivity within the Kubo-formula calculation. In this respect our strategy consists of a twofold way: First, we perform the renormalization group analysis and find how the distance between a pair of Weyl points evolves as a function of an energy scale or temperature. Second, introducing this information into the Boltzmann transport theory with chiral anomaly, we reveal the longitudinal negative magnetoconductivity as a function of both the applied magnetic field and temperature, given by

$$\sigma_L(B,T) \approx \sigma_D(T)[1 + \mathcal{C}_W(T)B^2]. \quad (5)$$

In particular, we find breakdown of B/T scaling

$$\Delta\sigma_L(B,T) \equiv \frac{\sigma_L(B,T) - \sigma_D(T)}{\sigma_D(T)} = \mathcal{C}_W T_0^{2(1+\eta)}\left(\frac{B}{T^{1+\eta}}\right)^2, \quad (6)$$

where η is a scaling exponent with $0 < \eta < 1$ and T_0 is an energy scale. We claim that this breakdown may be regarded to be a fingerprint of the interplay between disorder scattering and topological structure in a Weyl metal phase.

II. RENORMALIZATION FOR THE DISTANCE BETWEEN A PAIR OF WEYL POINTS VIA DISORDER-DRIVEN INTERVALLEY SCATTERING

A. Effective field theory for a Weyl metal phase with disorder: Replica theory

We start from an effective Hamiltonian density for a Weyl metal phase with time-reversal symmetry breaking

$$\mathcal{H}_B = \psi_B^\dagger(\boldsymbol{x})(v_B\boldsymbol{\alpha}\cdot(-\imath\nabla) + g_B\boldsymbol{B}\cdot\boldsymbol{\sigma}\otimes I_{2\times2})\psi_B(\boldsymbol{x}). \quad (7)$$

$\psi_B(\boldsymbol{x}) = (\psi_{BR}(\boldsymbol{x}),\psi_{BL}(\boldsymbol{x}))^T$ is a four-component Dirac-spinor field in a two-component Weyl-spinor field with right-left (R-L) chirality, and v_B is the velocity of such fermions. $\boldsymbol{B}$ is an externally applied magnetic field with a Lande-g factor g_B, splitting the Dirac band into a pair of Weyl bands (Fig. 1). $\boldsymbol{\alpha}$ is a four-by-four matrix, given by $\boldsymbol{\alpha} = \boldsymbol{\sigma}\otimes\sigma_z$, where $\boldsymbol{\sigma}$ is a Pauli matrix. The subscript B denotes bare, meaning that this effective Hamiltonian density is defined at an ultraviolet (UV) scale.

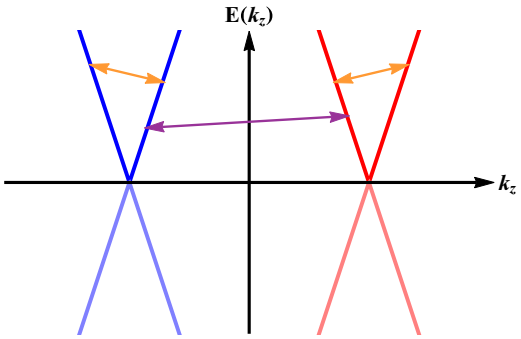

FIG. 1. A band structure of a Weyl metal phase, projected on the plane of $k_x = k_y = 0$. Here, the direction of an applied magnetic field is the z axis. Each band has definite chirality: -1 for the blue cone and $+1$ for the red cone. The orange arrows represent intravalley scattering while the purple arrow stands for intervalley scattering.

We consider two types of random potentials, introducing intravalley scattering $\psi_B^\dagger(\boldsymbol{x})V_B(\boldsymbol{x})\psi_B(\boldsymbol{x})$ and intervalley scattering $\psi_B^\dagger(\boldsymbol{x})U_B(\boldsymbol{x})(I_{2\times2}\otimes\sigma_x)\psi_B(\boldsymbol{x})$ into the effective Hamiltonian. Then, we obtain the following effective action

$$\begin{aligned} &S_B[\bar\psi_B(x),\psi_B(x);V_B(\boldsymbol{x}),U_B(\boldsymbol{x})] \\ &= \int d^4x\{\bar\psi_B(x)(\gamma^0\partial_0 + \imath v_B\gamma^k\partial_k + c_{B\mu}\gamma^\mu\gamma^5)\psi_B(x) \\ &\quad +\bar\psi_B(x)\gamma^0V_B(\boldsymbol{x})\psi_B(x) + \bar\psi_B(x)U_B(\boldsymbol{x})\psi_B(x)\} \end{aligned} \tag{8}$$

with $\bar\psi_B(x) \equiv \psi_B^\dagger(x)\gamma^0$. Here, γ matrices are given in the Weyl representation, for example, $\gamma^0 = I_{2\times2}\otimes\sigma_x$. A magnetic field is generalized to be a chiral gauge field $c_{B\mu} = (c_{B0}, c_{Bk} \equiv g_B B_k)$. x means space time, given by $x^\mu = (\tau,\boldsymbol{x})$, see the Appendix.

A physical observable in this system is measured as follows:

$$\begin{aligned} \langle O[\bar\psi_B(x),\psi_B(x)]\rangle &= \int \mathcal{D}V_B(\boldsymbol{x})\mathcal{D}U_B(\boldsymbol{x})P_B[V_B(\boldsymbol{x}),U_B(\boldsymbol{x})] \\ &\quad\times \frac{\int \mathcal{D}\bar\psi_B(x)\mathcal{D}\psi_B(x)O[\bar\psi_B(x),\psi_B(x)]e^{-S_{B0}[\bar\psi_B(x),\psi_B(x)]}e^{-\int d^4x\bar\psi_B(x)[\gamma^0V_B(\boldsymbol{x})+U_B(\boldsymbol{x})]\psi_B(x)}}{\int \mathcal{D}\bar\psi_B(x)\mathcal{D}\psi_B(x)e^{-S_{B0}[\bar\psi_B(x),\psi_B(x)]}e^{-\int d^4x\bar\psi_B(x)[\gamma^0V_B(\boldsymbol{x})+U_B(\boldsymbol{x})]\psi_B(x)}}, \end{aligned} \tag{9}$$

where the free part of the effective action is $S_{B0}[\bar\psi_B(x),\psi_B(x)] = \int d^4x\bar\psi_B(x)(\gamma^0\partial_0 + \imath v_B\gamma^k\partial_k + c_{B\mu}\gamma^\mu\gamma^5)\psi_B(x)$. Resorting to the replica trick and performing the average for disorder with the Gaussian distribution function of $P_B[V_B(\boldsymbol{x}),U_B(\boldsymbol{x})] = N_B\exp[-\frac{\int d^3\boldsymbol{x}V_B^2(\boldsymbol{x})}{2\Gamma_{BV}} - \frac{\int d^3\boldsymbol{x}U_B^2(\boldsymbol{x})}{2\Gamma_{BU}}]$, the above expression is reformulated as follows:

$$\begin{aligned} \langle O[\bar\psi_B(x),\psi_B(x)]\rangle &= \lim_{R\to0}\frac{1}{R}\sum_{a=1}^{R}\int \mathcal{D}\bar\psi_B^a(x)\mathcal{D}\psi_B^a(x)O\big[\bar\psi_B^a(x),\psi_B^a(x)\big] \\ &\quad\times\exp\left\{-\sum_{a=1}^{R}S_{B0}\big[\bar\psi_B^a(x),\psi_B^a(x)\big] - \sum_{b,c=1}^{R}S_{B\mathrm{dis}}\big[\bar\psi_B^b(x),\psi_B^b(x),\bar\psi_B^c(x),\psi_B^c(x)\big]\right\}. \end{aligned} \tag{10}$$

Here, N_B is a normalization constant and $\Gamma_{BV(U)}$ is a variance for the disorder distribution. As a result, the effective interaction term induced by disorder scattering is

$$\begin{aligned} S_{B\mathrm{dis}}\big[\bar\psi_B^b(x),\psi_B^b(x),\bar\psi_B^c(x),\psi_B^c(x)\big] &= -\int_0^\beta d\tau\int_0^\beta d\tau'\int d^3\boldsymbol{x}\frac{\Gamma_{BV}}{2}\bar\psi_B^b(\tau,\boldsymbol{x})\gamma^0\psi_B^b(\tau,\boldsymbol{x})\bar\psi_B^c(\tau',\boldsymbol{x})\gamma^0\psi_B^c(\tau',\boldsymbol{x}) \\ &\quad -\int_0^\beta d\tau\int_0^\beta d\tau'\int d^3\boldsymbol{x}\frac{\Gamma_{BU}}{2}\bar\psi_B^b(\tau,\boldsymbol{x})\psi_B^b(\tau,\boldsymbol{x})\bar\psi_B^c(\tau',\boldsymbol{x})\psi_B^c(\tau',\boldsymbol{x}). \end{aligned} \tag{11}$$

The effective field theory is given by $S_B[\bar\psi_B^a(x),\psi_B^a(x)] = S_{B0}[\bar\psi_B^a(x),\psi_B^a(x)] + S_{B\mathrm{dis}}[\bar\psi_B^b(x),\psi_B^b(x),\bar\psi_B^c(x),\psi_B^c(x)]$.

B. Renormalization group analysis: Role of intervalley scattering in the distance between a pair of Weyl point

In order to perform the renormalization group analysis within the dimensional regularization [9], we rewrite $S_B[\bar\psi_B^a(x),\psi_B^a(x)]$, the effective bare action of bare field variables in terms of $S_R[\bar\psi_R^a,\psi_R^a]$, the effective renormalized action of renormalized field variables with $S_{CT}[\bar\psi_R^a,\psi_R^a]$, counterterms of renormalized field variables

$$\begin{aligned} S_R\big[\bar\psi_R^a,\psi_R^a\big] &= \int d^{d+1}x\bar\psi_R^a(\gamma^0\partial_0 + v_R\imath\gamma^k\partial_k + c_{R0}\gamma^0\gamma^5 + c_{Rk}\gamma^k\gamma^5)\psi_R^a \\ &\quad -\int d\tau\int d\tau'\int d^d\boldsymbol{x}\frac{\Gamma_{RV}}{2}\big(\bar\psi_R^b\gamma^0\psi_R^b\big)_\tau\big(\bar\psi_R^c\gamma^0\psi_R^c\big)_{\tau'} - \int d\tau\int d\tau'\int d^d\boldsymbol{x}\frac{\Gamma_{RU}}{2}\big(\bar\psi_R^b\psi_R^b\big)_\tau\big(\bar\psi_R^c\psi_R^c\big)_{\tau'}, \\ S_{CT}\big[\bar\psi_R^a,\psi_R^a\big] &= \int d^{d+1}x\bar\psi_R^a\big(\delta_\psi^\omega\gamma^0\partial_0 + \delta_\psi^{\boldsymbol{k}}v_R\imath\gamma^k\partial_k + \delta_{c0}c_{R0}\gamma^0\gamma^5 + \delta_{\boldsymbol{c}}c_{Rk}\gamma^k\gamma^5\big)\psi_R^a - \int d\tau\int d\tau'\int d^d\boldsymbol{x} \\ &\quad\times\frac{\delta_{\Gamma V}\Gamma_{RV}}{2}\big(\bar\psi_R^b\gamma^0\psi_R^b\big)_\tau\big(\bar\psi_R^c\gamma^0\psi_R^c\big)_{\tau'} - \int d\tau\int d\tau'\int d^d\boldsymbol{x}\frac{\delta_{\Gamma U}\Gamma_{RU}}{2}\big(\bar\psi_R^b\psi_R^b\big)_\tau\big(\bar\psi_R^c\psi_R^c\big)_{\tau'}, \end{aligned} \tag{12}$$

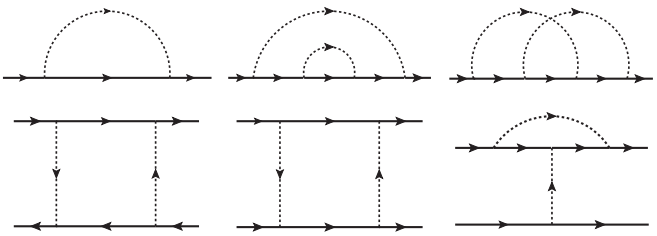

FIG. 2. Feynman's diagrams up to the two-loop order for self-energy corrections and the one-loop order for vertex corrections. The other diagrams disconnected to external lines or including fermion loops vanish identically in the replica limit of $R \to 0$. Here, we show quantum corrections only due to intravalley scattering, represented by single-dashed lines. In order to include intervalley scattering, we just replace single-dashed lines with double-dashed lines one by one according to our Feynman rules. This replacement results in another Fock-type diagram and three more diagrams each for rainbow-type, crossed-type, and vertex corrections.

where $S_B[\bar{\psi}^a_B,\psi^a_B] = S_R[\bar{\psi}^a_R,\psi^a_R] + S_{CT}[\bar{\psi}^a_R,\psi^a_R]$. It is straightforward to see how bare quantities are related with renormalized ones, given by

$$\begin{aligned}
&\psi^a_B = \left(Z^\omega_\psi\right)^{\frac{1}{2}}\psi^a_R, \quad v_B = Z^{\boldsymbol{k}}_\psi\left(Z^\omega_\psi\right)^{-1}v_R,\\
&c_{B0} = Z_{c0}\left(Z^\omega_\psi\right)^{-1}c_{R0}, \quad c_{Bk} = Z_{\boldsymbol{c}}\left(Z^\omega_\psi\right)^{-1}c_{Rk},\\
&\Gamma_{BV} = Z_{\Gamma V}\left(Z^\omega_\psi\right)^{-2}\Gamma_{RV}, \quad \Gamma_{BU} = Z_{\Gamma U}\left(Z^\omega_\psi\right)^{-2}\Gamma_{RU},
\end{aligned} \tag{13}$$

where $Z^\omega_\psi = 1+\delta^\omega_\psi$, $Z^{\boldsymbol{k}}_\psi = 1+\delta^{\boldsymbol{k}}_\psi$, $Z_{c0} = 1+\delta_{c0}$, $Z_{\boldsymbol{c}} = 1+\delta_{\boldsymbol{c}}$, $Z_{\Gamma V} = 1+\delta_{\Gamma V}$, and $Z_{\Gamma U} = 1+\delta_{\Gamma U}$.

Dimensional analysis gives $\dim[\Gamma] = 2-d$. In this respect we perform the dimensional regularization in $d = 2+\varepsilon$ where ε, a small parameter to control the present renormalization group analysis, will be analytically continued to $\varepsilon = 1$ in the end. Performing the standard procedure for the renormalization group analysis, we find renormalization group equations, where both vertex and self-energy corrections are introduced self-consistently. See Fig. 2, where all quantum corrections are shown as Feynman's diagrams up to the two-loop order for self-energy corrections and the one-loop order for vertex corrections. All details are shown in the Appendix. As a result, we find counterterms with

$$\begin{aligned}
\delta^\omega_\psi &= \frac{\Gamma_V+\Gamma_U}{2\pi\varepsilon} - \frac{5\Gamma_V^2+12\Gamma_V\Gamma_U+7\Gamma_U^2}{48\pi^2\varepsilon},\\
\delta_{\boldsymbol{c}} &= \frac{\Gamma_V^2-\Gamma_U^2}{16\pi^2\varepsilon}, \quad \delta_{\Gamma V} = \frac{\Gamma_V+\Gamma_U}{2\pi\varepsilon},\\
\delta_{\Gamma U} &= -\frac{\Gamma_V+\Gamma_U}{2\pi\varepsilon}.
\end{aligned} \tag{14}$$

Inserting these divergent coefficients into equations (13) and performing derivatives with respect to an energy scale for renormalization given by $\ln M$, we find renormalization group equations

$$\begin{aligned}
\frac{d\Gamma_V}{d\ln M} &= \Gamma_V - \frac{a_\Gamma}{3}\Gamma_V(\Gamma_V+\Gamma_U)\\
&\quad + b_\Gamma\Gamma_V(\Gamma_V+\Gamma_U)(c_\Gamma\Gamma_V+\Gamma_U),\\
\frac{d\Gamma_U}{d\ln M} &= \Gamma_U - a_\Gamma\Gamma_U(\Gamma_V+\Gamma_U)\\
&\quad + b_\Gamma\Gamma_U(\Gamma_V+\Gamma_U)(c_\Gamma\Gamma_V+\Gamma_U),\\
\frac{dc_k}{d\ln M} &= c_k[-1 - a_{\boldsymbol{c}}(\Gamma_V+\Gamma_U)\\
&\quad + b_{\boldsymbol{c}}(\Gamma_V+\Gamma_U)(2\Gamma_V+\Gamma_U)],
\end{aligned} \tag{15}$$

where positive numerical constants are given by

$$a_\Gamma = \frac{3}{2\pi}, \quad b_\Gamma = \frac{7}{24\pi^2}, \quad c_\Gamma = \frac{5}{7}, \quad a_{\boldsymbol{c}} = \frac{1}{2\pi}, \quad b_{\boldsymbol{c}} = \frac{1}{12\pi^2}.$$

Scaling analysis in the tree level suggests that both channels of impurity scattering are irrelevant in the low-energy limit because of the pseudogap density of states. In the one-loop order Fock diagrams contribute to the wave-function renormalization constant. Particle-hole and particle-particle channel diagrams in the vertex are canceled to each other while vertex-correction diagrams give two distinct effects for impurity scattering: The intervalley scattering is strengthened while the intravalley scattering is weakened. This discrepancy turns out to reflect the sign difference in the dispersions of two chiral modes. Combined with the wave-function renormalization from Fock diagrams, there appears a disparity, that is, the strength of intervalley scattering is three times larger than that of intravalley scattering [21]. Enhancement of both impurity scattering channels stops after two-loop corrections are introduced into the self-energy. Especially, rainbow diagrams contribute to the wave-function renormalization constant, identified with screening for impurity scattering. Crossed diagrams renormalize the chiral-gauge field but effects by both impurity scattering channels appear in an opposite way again: The intervalley scattering increases the strength of the chiral gauge field while the intravalley scattering decreases it.

Figure 3 shows renormalization group flows for physical parameters according to Eq. (15). In the plane of (Γ_V,Γ_U), we find two stable fixed points corresponding to two phases of a disordered Weyl metal state, and one unstable fixed point corresponding to the phase transition point between two phases: (i) The stable fixed point of $(0,\Gamma_0)$ with $\Gamma_0 = 0$ represents a clean Weyl metal phase, protected for the case of weak disorder by the pseudogap density of states of the Weyl metal state. (ii) The stable fixed point of $(0,\Gamma_2)$ with $\Gamma_2 = \frac{a_\Gamma+\sqrt{a_\Gamma^2-4b_\Gamma}}{2b_\Gamma} \simeq 13.68$ is identified with a diffusive Weyl metal phase, analogous to the diffusive Fermi-liquid fixed point of a conventional metallic phase [22]. (iii) The unstable fixed point of $(0,\Gamma_1)$ with $\Gamma_1 = \frac{a_\Gamma-\sqrt{a_\Gamma^2-4b_\Gamma}}{2b_\Gamma} \simeq 2.09$ denotes a critical point to separate the diffusive Weyl metal phase from the clean Weyl metal state, the existence of which originates from the pseudogap density of states. Interestingly, all these fixed points lie at the line of $\Gamma_V = 0$, which means that intervalley scattering shows dominant effects over intravalley scattering for the low-energy physics in the disordered Weyl metallic state. Naively, one may suspect that their roles are similar because of the similarity of their renormalization group equations. However, the magnitude of the one-loop correction for Γ_U is three times larger than that for Γ_V, and thus, the renormalization group flow of (Γ_V,Γ_U) is overwhelmed by

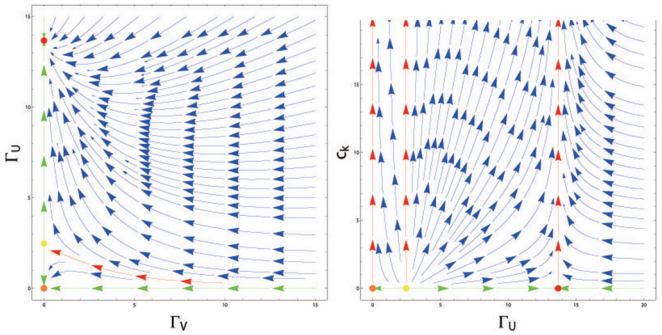

FIG. 3. Renormalization group flows for physical parameters. In the plane of (Γ_V,Γ_U) (left), there are two stable fixed points and one unstable fixed point: (i) The stable fixed point of $(0,\Gamma_0)$ with $\Gamma_0 = 0$ represents a clean Weyl metal phase, protected for the case of weak disorder by the pseudogap density of states of the Weyl metal state. (ii) The stable fixed point of $(0,\Gamma_2)$ with $\Gamma_2 = \frac{a_\Gamma+\sqrt{a_\Gamma^2-4b_\Gamma}}{2b_\Gamma} \simeq 13.68$ is identified with a diffusive Weyl metal phase, analogous to the diffusive Fermi-liquid fixed point of a conventional metallic phase. (iii) The unstable fixed point of $(0,\Gamma_1)$ with $\Gamma_1 = \frac{a_\Gamma-\sqrt{a_\Gamma^2-4b_\Gamma}}{2b_\Gamma} \simeq 2.09$ denotes a critical point to separate the diffusive Weyl metal phase from the clean Weyl metal state, the existence of which originates from the pseudogap density of states. In the plane of (Γ_U,c_k) (right), the renormalization group flow shows a runaway behavior for c_k, implying that the Weyl metallic state is stabilized even in the presence of disorder scattering. This runaway flow should stop at a certain energy scale if the Brillouin zone is taken into account in the effective field theory.

Γ_U. As a result, there is no chance by which Γ_V has a nontrivial fixed-point value. Detailed analysis of this issue is given in the Appendix (Fig. 16).

In order to figure out how the distance between the pair of Weyl points renormalizes as a function of an energy scale, we focus on renormalization group equations for Γ_U and c_k at $\Gamma_V = 0$

$$\frac{d\Gamma_U}{d\ln M} = \Gamma_U - a_\Gamma\Gamma_U^2 + b_\Gamma\Gamma_U^3 \tag{16}$$

$$\frac{dc_k}{d\ln M} = c_k\left[-1 - a_{\boldsymbol{c}}\Gamma_U + b_{\boldsymbol{c}}\Gamma_U^2\right]. \tag{17}$$

It is straightforward to solve the first equation and find an approximate solution for Γ_U near each fixed point at $\Gamma_V = 0$. Inserting such fixed-point solutions into the second equation, we uncover how the distance between the pair of Weyl points evolves as a function of temperature

$$c_k(T) = c_k(T_0)\left(\frac{T_0}{T}\right)^{\lambda_{\boldsymbol{c},fn}}, \tag{18}$$

where the energy scale M has been replaced with temperature T. Critical exponents of $\lambda_{\boldsymbol{c},fn}$ are found to be

$$\lambda_{\boldsymbol{c},f0} = 1 + a_{\boldsymbol{c}}\Gamma_0 - b_{\boldsymbol{c}}\Gamma_0^2 = 1 \tag{19}$$

$$\lambda_{\boldsymbol{c},f1} = 1 + a_{\boldsymbol{c}}\Gamma_1 - b_{\boldsymbol{c}}\Gamma_1^2 \simeq 1.34 \tag{20}$$

$$\lambda_{\boldsymbol{c},f2} = 1 + a_{\boldsymbol{c}}\Gamma_2 - b_{\boldsymbol{c}}\Gamma_2^2 \simeq 1.60. \tag{21}$$

It turns out that the distance between a pair of Weyl points increases to reach infinity, regarded to be beyond the perturbative renormalization group analysis. However, the infinity should be considered as an artifact of the continuum approximation. If the Brillouin zone is taken into account in the effective field theory, there must be a maximum of the distance within the Brillouin zone. In this respect it is natural to modify the above scaling solution as follows:

$$c_k(T) = c_k(T_0)\left(\frac{T_0}{T+T_M}\right)^{\lambda_{\boldsymbol{c},fn}}, \tag{22}$$

where T_M is a cutoff scale in the low-energy limit. It is interesting to notice that disorder scattering changes the temperature-dependent exponent of c_k. Intervalley scattering gives rise to fast enhancement of the distance between a pair of Weyl points at low temperatures. This looks counterintuitive, where antiscreening instead of screening arises from intervalley scattering.

One may criticize that the renormalization group analysis does not take into account the role of orbital effects driven by external magnetic fields. Actually, the formation of Landau levels plays an essential role in the previous study of Ref. [14]. When applied magnetic fields are strong enough, given by the condition of $\hbar\omega_c \gg \mu$, where ω_c is the cyclotron frequency and μ is the chemical potential, the formation of Landau levels plays a central role in the Weyl metallic state. The zeroth Landau level opens a one-dimensional channel, where the chiral anomaly is realized in a one-dimensional way [9]. On the other hand, when the chemical potential is much larger than the applied magnetic field, i.e., $\hbar\omega_c \ll \mu$, effects of Landau levels can be neglected as discussed in the previous study [16]. Then, the Zeeman term plays an essential role in the chiral anomaly. Recall that the chiral gauge field is nothing but the applied magnetic field, identified with the spatial gradient of the θ coefficient of the topological-in-origin θ term.

III. TWO-PARAMETER SCALING THEORY FOR THE LONGITUDINAL MAGNETOCONDUCTIVITY OF A DISORDERED WEYL METAL PHASE WITHIN BOLTZMANN TRANSPORT THEORY

The question to address in this study is to find a scaling theory for the longitudinal magnetoconductivity. As discussed in the introduction, not only the Drude conductivity but also the distance between a pair of Weyl points or the spatial gradient of the inhomogeneous $\theta(\boldsymbol{r})$ coefficient in the topological-in-origin $\boldsymbol{E}\cdot\boldsymbol{B}$ term should be taken into account for the longitudinal magnetoconductivity in the Weyl metal phase. This situation is analogous to that of a plateau-plateau transition in the integer quantum Hall effect: Not only the Drude conductivity but also the Hall conductivity, a topological θ term, should be considered on equal footing in order to describe such a quantum phase transition involved with Anderson localization. In this respect we call the scaling theory for the longitudinal magnetoconductivity of a disordered Weyl metal phase two-parameter scaling theory as the Anderson localization transition in the case of the quantum Hall effect.

Previously, we found $\Gamma_U(T)$ and $c(T)$, based on the perturbative renormalization group analysis, where $\Gamma_U(T)$

gives the Drude conductivity and $c(T)$ describe the enhancement of the longitudinal magnetoconductivity. More precisely, we can address renormalization effects of the longitudinal magnetoconductivity based on the Boltzmann transport theory for a Weyl metal phase [17,23]

$$\frac{\partial n_\chi(\boldsymbol{p};\boldsymbol{r},t)}{\partial t} + \dot{\boldsymbol{r}}_\chi \cdot \nabla_{\boldsymbol{r}} n_\chi(\boldsymbol{p};\boldsymbol{r},t) + \dot{\boldsymbol{p}}_\chi \cdot \nabla_{\boldsymbol{p}} n_\chi(\boldsymbol{p};\boldsymbol{r},t) = I_{\rm coll}[n_\chi(\boldsymbol{p};\boldsymbol{r},t)]. \quad (23)$$

Here, $n_\chi(\boldsymbol{p};\boldsymbol{r},t)$ is the distribution function at a chiral Fermi surface denoted by $\chi = \pm$, where $\boldsymbol{p}$ is the relative momentum of a particle-hole pair near the chiral Fermi surface, and $\boldsymbol{r}$ and t are the center of mass position and time of the particle-hole pair.

$\dot{\boldsymbol{r}}_\chi$ and $\dot{\boldsymbol{p}}_\chi$ represent the change of position and momentum with respect to time, classically described and given by the so-called modified Drude model [24,25]

$$\dot{\boldsymbol{x}}_F^\chi = \boldsymbol{v}_F^\chi + \dot{\boldsymbol{p}}_F^\chi \times \boldsymbol{\mathcal{B}}_F^\chi,$$
$$\dot{\boldsymbol{p}}_F^\chi = \boldsymbol{E} + \dot{\boldsymbol{x}}_F^\chi \times \boldsymbol{B}. \quad (24)$$

$\boldsymbol{\mathcal{B}}_F^\chi$ represents a momentum-space magnetic field on the chiral Fermi surface, resulting from a momentum-space magnetic charge χ enclosed by the chiral Fermi surface. We would like to recall that the Berry curvature does not appear on the normal Fermi surface that does not enclose a band-touching point. As a result, we reproduce the Drude model with $\boldsymbol{\mathcal{B}}_F^\chi = 0$. It is essential to realize the following relation between the applied magnetic field and the distance between the pair of Weyl points

$$\boldsymbol{B} \to g^{-1}\boldsymbol{c}(T). \quad (25)$$

It is straightforward to solve these coupled equations, the solution of which is

$$\dot{\boldsymbol{x}}_F^\chi \approx G_3^\chi(T)\big[\boldsymbol{v}_F^\chi + \boldsymbol{E}\times\boldsymbol{\mathcal{B}}_F^\chi + g^{-1}\big(\boldsymbol{\mathcal{B}}_F^\chi\cdot\boldsymbol{v}_F^\chi\big)\boldsymbol{c}(T)\big],$$
$$\dot{\boldsymbol{p}}_F^\chi \approx G_3^\chi(T)\big[\boldsymbol{E} + g^{-1}\boldsymbol{v}_F^\chi\times\boldsymbol{c}(T) + g^{-1}\big(\boldsymbol{E}\cdot\boldsymbol{c}(T)\big)\boldsymbol{\mathcal{B}}_F^\chi\big], \quad (26)$$

where $G_3^\chi = (1 + g^{-1}\boldsymbol{\mathcal{B}}_F^\chi\cdot\boldsymbol{c}(T))^{-1}$ is a volume factor of the modified phase space with a pair of momentum-space magnetic charges $\chi = \pm$. The role of anomalous electromagnetic-field-dependent terms are well known in anomalous transport phenomena: (i) The second term of $\boldsymbol{E}\times\boldsymbol{\mathcal{B}}_F^\chi$ in the first equation is responsible for the anomalous Hall effect, the Hall effect without an applied magnetic field due to an emergent magnetic field referred to as Berry curvature in the momentum space [26–28]. (ii) The third term of $g^{-1}(\boldsymbol{\mathcal{B}}_F^\chi\cdot\boldsymbol{v}_F^\chi)\boldsymbol{c}(T)$ in the first equation gives rise to the so called chiral magnetic effect that dissipationless electric currents are driven by applied magnetic fields in the limit of vanishing applied electric fields, proportional to the distance between the pair of Weyl points or applied magnetic fields [29–34]. (iii) The third term of $g^{-1}(\boldsymbol{E}\cdot\boldsymbol{c}(T))\boldsymbol{\mathcal{B}}_F^\chi$ in the second equation causes the gauge anomaly for electrons on each chiral Fermi surface that gauge or electric currents on each chiral Fermi surface are not conserved [14–17,23,30,31,35–42]. Of course, the breakdown of the gauge symmetry should be cured when total electric currents are considered, but chiral electric currents are still not conserved, referred to as chiral anomaly.

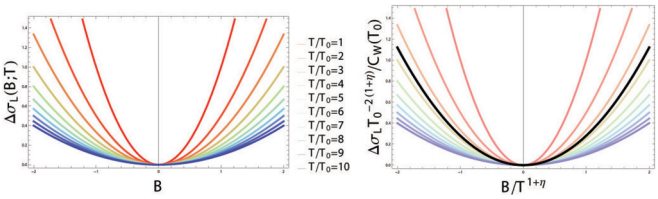

FIG. 4. Scaling theory for the longitudinal magnetoconductivity. The longitudinal magnetoconductivity is enhanced to be proportional to B^2, the distance between the pair of Weyl point as a result of the chiral anomaly. The distance between the pair of Weyl points is renormalized to increase as temperature is reduced, which makes the degree of enhancement become larger (left). These longitudinal transport coefficients are collapsed into a single universal curve, described by Eq. (30) (right).

The collision part is given by

$$I_{\rm coll}[\delta n_\chi(\boldsymbol{p};\boldsymbol{r},t)] = -\frac{n_\chi(\boldsymbol{p};\boldsymbol{r},t) - n_\chi^{\rm eq}(\boldsymbol{p})}{\tau_{\rm intra}(T)} - \frac{n_\chi(\boldsymbol{p};\boldsymbol{r},t) - n_{-\chi}(\boldsymbol{p};\boldsymbol{r},t)}{\tau_{\rm inter}(T)}. \quad (27)$$

The first term describes the intravalley scattering, and the second represents the intervalley scattering. In this respect both scattering rates of $1/\tau_{\rm intra}(T)$ and $1/\tau_{\rm intra}(T)$ correspond to $\Gamma_V(T)$ and $\Gamma_U(T)$, respectively.

Considering homogeneity of the Weyl metal phase under constant electric fields in the dc limit, we are allowed to solve $\dot{\boldsymbol{p}}_\chi\cdot\nabla_{\boldsymbol{p}} n_\chi(\boldsymbol{p}) = I_{\rm coll}[n_\chi(\boldsymbol{p})]$. As a result, we find a two-parameter scaling theory for the longitudinal magnetoconductivity in a disordered Weyl metal phase

$$\sigma_L(B,T) = \sigma_D(B,T)(1 + \text{const.}[c(B,T)]^2), \quad (28)$$

where $\sigma_D(B,T)$ is the Drude conductivity inversely proportional to $\Gamma_U(T)$ and $c(B,T)$ is the distance between a pair of Weyl points.

Rewriting the distance between the pair of Weyl points as $c(B,T) \equiv C_W^{1/2}(T)B$, we consider

$$\Delta\sigma_L(B,T) \equiv \frac{\sigma_L(B,T) - \sigma_D(B,T)}{\sigma_D(B,T)} = C_W(T)B^2 \quad (29)$$

for the universal scaling relation. More explicitly, inserting $C_W(T) = C_W(T_0)[T_0/(T + T_M)]^{-2\lambda_{c,fn}}$ into the above, we find

$$\frac{T_0^{-2(1+\eta_n)}\Delta\sigma_L(B,T)}{C_W(T_0)} = \left(\frac{B}{[T + T_M]^{1+\eta_n}}\right)^2, \quad (30)$$

where anomalous dimensions are given by $\eta_0 = 0, \eta_1 = 0.34$, and $\eta_2 = 0.60$, respectively, for each fixed point.

Figure 4 shows the longitudinal magnetoconductivity, enhanced to be proportional to B^2, the square of the distance between the pair of Weyl points, at each temperature. Our renormalization group analysis confirms that the distance between the pair of Weyl points is renormalized to increase, lowering temperature, i.e., $C_W(T_H) < C_W(T_L)$ with $T_H > T_L$. As a result, the degree of enhancement becomes larger as temperature is reduced (left). Interestingly, these longitudinal transport coefficients turn out to be collapsed into a single universal curve, described by Eq. (30) (right).

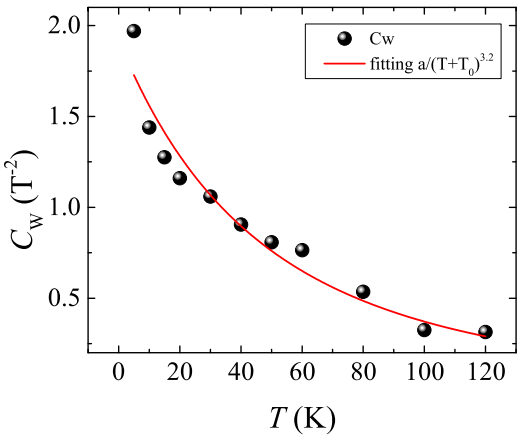

FIG. 5. Comparison between the theoretical prediction and an experimental data of $Bi_{1-x}Sb_x$ with $x = 3 \sim 4\%$. Black spheres represent experimental data [8,43] and the red line denotes the theoretical prediction, given by $\frac{C_W(T)}{C_W(T_0)T_0^{-2\lambda_{c,f2}}} = \frac{1}{(T+T_M)^{-2\lambda_{c,f2}}}$. Here, we obtain $\frac{C_W(T)}{C_W(T_0)T_0^{-2\lambda_{c,f2}}} = 1.7 * 10^7\ \mathrm{K}^{2\lambda_{c,f2}}$ and $T_M = 149$ K with $\lambda_{c,f2} = -1.6$ at the diffusive fixed point.

Figure 5 shows the comparison between $C_W(T)$ from an experimental data of $Bi_{1-x}Sb_x$ with $x = 3 \sim 4\%$ and that from our renormalization group analysis [8,43]. Experimentally, the enhancement coefficient $C_W(T)$ can be found from fitting the experimental data with Eq. (5) at a given temperature, where the Drude part is replaced with a transport coefficient of weak antilocalization corrections and additional contributions, which have nothing to do with Weyl points, are also introduced [15]. Repeating this fitting procedure for various temperatures, we obtain the temperature dependence of $C_W(T)$. The comparison between the experimental $C_W(T)$ and the renormalization group analysis Eq. (30) looks appealing.

IV. DISCUSSION AND CONCLUSION

The original motivation of the present study is to reveal the existence of a topological phase transition from a Weyl metal phase to a normal metal state as a function of the strength of disorder and temperature. Our physical picture for this phase transition is as follows. Disorder scattering, in particular, intervalley scattering is expected to kill the nature of the Weyl metallic phase since it induces mixing of chirality. We recall that the intervalley scattering appears as an effective random-mass term. If $\bar{\psi}(x)\psi(x)$ has a nontrivial vacuum expectation value, i.e., $\langle\bar{\psi}(x)\psi(x)\rangle \neq 0$, expected to realize in the case of sufficiently strong disorder, the chiral symmetry breaks down even at the classical level and the chiral anomaly loses the physical meaning. As a result, we speculate that the distance between the pair of Weyl points renormalizes to vanish. A diffusive normal metallic state would be realized in the case of sufficiently strong disorder. Since this phase transition is not involved with symmetry breaking, it is identified with a topological phase transition.

This topological phase transition may be translated into Peccei-Quinn symmetry breaking in the context of dynamical generation of axions [44,45]. In order to realize the Peccei-Quinn symmetry breaking, there must be a scalar field. When the scalar field does not have its vacuum expectation value, any value of the θ angle can be canceled by the Peccei-Quinn transformation. On the other hand, the Peccei-Quinn symmetry breaking occurs when the scalar field has its vacuum expectation value. As a result of the continuous symmetry breaking, there exists a Goldstone boson field, referred to as an axion field. When the Peccei-Quinn symmetry is exact and, thus, the axion field is massless, any value of the θ angle can be still canceled by the Peccei-Quinn transformation. However, there are instanton excitations, which do not allow the Peccei-Quinn symmetry not to be exact, giving rise to a mass term in the axion dynamics. Then, the vacuum angle is fixed to be $\theta = 0$, minimizing the energy of the system. In the present situation the corresponding scalar field results from the Hubbard-Stratonovich transformation of the random-mass term in the replica effective field theory, conventionally referred to as Q_{ab}, where a and b denote the replica index. However, there are two different aspects between the possible topological phase transition and the Peccei-Quinn symmetry breaking in high-energy physics: (i) The vacuum angle is given by an inhomogeneous function of position while its gradient identified with a chiral gauge field is a constant. (ii) There are no instanton-type excitations in the Weyl metal phase. This direction of research would be an interesting future task.

Unfortunately, the perturbative renormalization group analysis fails to access such an unstable fixed point, identified with the quantum critical point of the topological phase transition. In this respect the naming of the two-parameter scaling theory is not satisfactory in our opinion, basically motivated from the analogy with the plateau-plateau transition in the integer quantum Hall effect. However, it turns out that the longitudinal magnetoconductivity is governed by both parameters of the Drude conductivity and the distance between the pair of Weyl points, renormalized by intervalley scattering, essentially analogous to σ_{xx} and σ_{xy} in the quantum Hall effect, respectively. In this respect we may call what we performed two-parameter scaling theory for the longitudinal magnetoconductivity in a disordered Weyl metal phase.

An unexpected result is breakdown of the B/T scaling behavior near the diffusive fixed point although it is fulfilled near the clean fixed point. Actually, we could verify this prediction, comparing the proposed formula Eq. (30) of the two-parameter scaling theory with $C_W(T)$ in the experimental data of $Bi_{1-x}Sb_x$ with $x = 3 \sim 4\%$. Here, we took into account modifying the original renormalization group analysis, introducing a cutoff scale into the equation for the distance between the pair of Weyl points as Eq. (22), in order to prohibit the divergence of the length scale within the Brillouin zone. This breakdown may be regarded to be a fingerprint of the interplay between disorder scattering and topological structure in a Weyl metal phase.

In this study interference effects due to multiple scattering have not been taken into account. Such localization effects may be described, considering a two-particle Green's function instead of a single-particle propagator. The construction of self-consistent equations for two-particle Green's functions in Weyl metals is to generalize the previous study of Ref. [46] in normal metals, introducing not only the information of the Berry curvature but also the physics of the chiral anomaly into such self-consistent equations. We suspect that this derivation

is challenging since high-energy electrons should be integrated out in order to realize the effect of the chiral anomaly in the dynamics of low-energy electrons near a Fermi surface. We recall that this point was discussed sincerely in Ref. [20]. On the other hand, we may consider a phenomenological approach, where localization corrections are introduced into coupled Boltzmann equations directly [15,17]. Within this formulation, renormalization effects in the distance between a pair of Weyl points should be taken into account, as performed in this study.

ACKNOWLEDGMENTS

This study was supported by the Ministry of Education, Science, and Technology (Grants No. NRF-2015R1C1A1A01051629 and No. 2011-0030046) of the National Research Foundation of Korea (NRF) and by the TJ Park Science Fellowship of the POSCO TJ Park Foundation. This work was also supported by the POSTECH Basic Science Research Institute Grant (2015). We appreciate fruitful discussions in the APCTP workshop on Delocalisation Transitions in Disordered Systems.

APPENDIX A: MODEL HAMILTONIAN

A minimal model for a Weyl metal state is given by

$$\mathcal{H} = \psi^\dagger(\boldsymbol{x})(v\boldsymbol{\alpha}\cdot(-\imath\boldsymbol{\nabla}) - \mu + g\boldsymbol{B}\cdot\boldsymbol{\sigma}\otimes I_{2\times2})\psi(\boldsymbol{x}).$$

$\psi = (\psi_R,\psi_L)^T$ is a four-component Dirac-spinor field in a two-component Weyl-spinor field with right-left (R-L) chirality, and v is the velocity of such fermions. μ is an electron chemical potential. $\boldsymbol{B}$ is an externally applied magnetic field with a Lande-g factor g. $\boldsymbol{\alpha}$ is a four-by-four matrix, given by $\boldsymbol{\alpha} = \boldsymbol{\sigma}\otimes\sigma_z$, where $\boldsymbol{\sigma}$ is a Pauli matrix.

First, we look into a band structure. This block-diagonal matrix can be diagonalized as

$$\mathcal{H}_{\boldsymbol{k}} = \phi^\dagger_{\boldsymbol{k}}(|v\boldsymbol{k}+g\boldsymbol{B}|\sigma_z\otimes P_+ - |v\boldsymbol{k}-g\boldsymbol{B}|\sigma_z\otimes P_- - \mu)\phi_{\boldsymbol{k}},$$

where $P_+ = \left(\begin{smallmatrix}1&0\\0&0\end{smallmatrix}\right)$ and $P_- = \left(\begin{smallmatrix}0&0\\0&1\end{smallmatrix}\right)$ are projection matrices, and $\phi_{\boldsymbol{k}} = U_{\boldsymbol{k}}\psi_{\boldsymbol{k}}$ is an eigenstate. The unitary matrix varying with $\boldsymbol{k}$ is given by

$$U_{\boldsymbol{k}} = \begin{pmatrix}\cos\frac{\zeta_+}{2} & \sin\frac{\zeta_+}{2}e^{-\imath\eta_+}\\ -\sin\frac{\zeta_+}{2}e^{\imath\eta_+} & \cos\frac{\zeta_+}{2}\end{pmatrix}\otimes P_+ + \begin{pmatrix}\cos\frac{\zeta_-}{2} & \sin\frac{\zeta_-}{2}e^{-\imath\eta_-}\\ -\sin\frac{\zeta_-}{2}e^{\imath\eta_-} & \cos\frac{\zeta_-}{2}\end{pmatrix}\otimes P_-,$$

where $\zeta_\pm$ ($\eta_\pm$) is the polar (azimuthal) angle of $\boldsymbol{k}\pm\frac{g}{v}\boldsymbol{B}$, respectively. If we draw a band structure along some momentum line, for example, $\boldsymbol{k} = (0,0,k_z)$, then we obtain a pair of Weyl cones as shown in Fig. 1.

Second, we consider two types of random potentials, i.e., intravalley scattering and intervalley scattering, given by

$$\begin{aligned}&\psi^\dagger_R(\boldsymbol{x})V(\boldsymbol{x})\psi_R(\boldsymbol{x}) + \psi^\dagger_L(\boldsymbol{x})V(\boldsymbol{x})\psi_L(\boldsymbol{x})\\ &\quad= \psi^\dagger(\boldsymbol{x})V(\boldsymbol{x})\psi(\boldsymbol{x}),\\ &\psi^\dagger_R(\boldsymbol{x})U(\boldsymbol{x})\psi_L(\boldsymbol{x}) + \psi^\dagger_R(\boldsymbol{x})U(\boldsymbol{x})\psi_L(\boldsymbol{x})\\ &\quad= \psi^\dagger(\boldsymbol{x})U(\boldsymbol{x})(I_{2\times2}\otimes\sigma_x)\psi(\boldsymbol{x}),\end{aligned}$$

where $V(\boldsymbol{x})$ and $U(\boldsymbol{x})$ are disorder potentials for intravalley scattering and intervalley scattering, respectively.

Now, the effective action is

$$\begin{aligned}&S[\psi^\dagger,\psi;V,U]\\ &\quad= \int_0^\beta d\tau\int d^3\boldsymbol{x}\,\psi^\dagger(\tau,\boldsymbol{x})\{\partial_\tau + v\boldsymbol{\alpha}\cdot(-\imath\nabla) - \mu\\ &\qquad+ g\boldsymbol{B}\cdot\boldsymbol{\sigma}\otimes I_{2\times2} + V(\boldsymbol{x}) + U(\boldsymbol{x})I_{2\times2}\otimes\sigma_x\}\psi(\tau,\boldsymbol{x}),\end{aligned}$$

where the corresponding free energy is given by $F[V,U] = -T\ln\int\mathcal{D}\psi^\dagger\mathcal{D}\psi e^{-S[\psi^\dagger,\psi;V,U]}$ in a given configuration of random potentials. We represent this effective action in terms of γ matrices in the Weyl representation

$$\gamma^0 = I_{2\times2}\otimes\sigma_x,\quad \gamma^k = \gamma^0(-\alpha_k) = \sigma_k\otimes\imath\sigma_y(k=1,2,3),$$
$$\gamma^5 = \imath\gamma^0\gamma^1\gamma^2\gamma^3 = -I_{2\times2}\otimes\sigma_z.$$

Then, we reach the following expression:

$$\begin{aligned}&S[\bar\psi,\psi;V,U]\\ &\quad= \int d^4x\{\bar\psi(x)(\gamma^0\partial_0 + \imath v\gamma^k\partial_k - \mu\gamma^0 + c_\mu\gamma^\mu\gamma^5)\psi(x)\\ &\qquad+\bar\psi(x)\gamma^0V(\boldsymbol{x})\psi(x) + \bar\psi(x)U(\boldsymbol{x})\psi(x)\}\end{aligned}$$

with an adjoint spinor-field $\bar\psi\equiv\psi^\dagger\gamma^0$, where we introduced $c_k\equiv gB_k$ ($k=1,2,3$) with time component c_0. The space time of x is $x^\mu = (\tau,\boldsymbol{x})$ and other four-vectors are defined, similarly. For example, the four-momentum is $p^\mu = (p^0,\boldsymbol{p})$ with $p^0 = -\imath\omega_n$. Since the action has been formulated in the imaginary time, it is defined on the Euclidean geometry as shown by $p^\mu p_\mu = -\omega_n^2 - \boldsymbol{p}^2$.

APPENDIX B: EFFECTIVE FIELD THEORY FOR RENORMALIZATION GROUP ANALYSIS

1. Disorder average

We define the free part of the effective action as

$$S_0[\bar\psi,\psi] = \int d^4x\,\bar\psi(x)(\gamma^0\partial_0 + \imath v\gamma^k\partial_k - \mu\gamma^0 + c_\mu\gamma^\mu\gamma^5)\psi(x).$$

Then, a physical observable is measured as follows

$$\langle O(\bar\psi,\psi)\rangle = \int\mathcal{D}V\mathcal{D}U\,P[V,U]\frac{\int\mathcal{D}\bar\psi\mathcal{D}\psi\,O(\bar\psi,\psi)e^{-S_0[\bar\psi,\psi]}e^{-\int d^4x\bar\psi(x)[\gamma^0V(\boldsymbol{x})+U(\boldsymbol{x})]\psi(x)}}{\int\mathcal{D}\bar\psi\mathcal{D}\psi e^{-S_0[\bar\psi,\psi]}e^{-\int d^4x\bar\psi(x)[\gamma^0V(\boldsymbol{x})+U(\boldsymbol{x})]\psi(x)}}.$$

This can be reformulated as

$$\langle O(\bar{\psi},\psi)\rangle = \int \mathcal{D}V\mathcal{D}U\, P[V,U]\frac{\delta}{\delta J}\bigg|_{J=0} \ln Z[V,U,J],$$
$$Z[V,U,J] = \int \mathcal{D}\bar{\psi}\mathcal{D}\psi e^{-S_0[\bar{\psi},\psi]} e^{-\int d^4x\bar{\psi}(x)[\gamma^0 V(\boldsymbol{x})+U(\boldsymbol{x})]\psi(x)+\int d^4x J(x)O[\bar{\psi}(x),\psi(x)]},$$

where $J(x)$ is a source field coupled to an operator $O(\bar{\psi},\psi)$, locally.

In order to perform the averaging procedure for disorders, we resort to the replica trick of $\ln Z = \lim_{R\to 0}\frac{Z^R-1}{R}$

$$\langle O(\bar{\psi},\psi)\rangle = \lim_{R\to 0}\int \mathcal{D}V\mathcal{D}U\, P[V,U]\frac{\delta}{\delta J}\bigg|_{J=0}\frac{Z^R[V,U,J]-1}{R},$$

where the replicated partition function is

$$Z^R[V,U,J] = \int \mathcal{D}\bar{\psi}^a\mathcal{D}\psi^a \exp\left[-\sum_{a=1}^R S_0[\bar{\psi}^a,\psi^a] - \sum_{a=1}^R\int d^4x\bar{\psi}^a(x)(\gamma^0 V(\boldsymbol{x})+U(\boldsymbol{x}))\psi^a(x) + \int d^4x J(x)\sum_{a=1}^R O(\bar{\psi}^a,\psi^a)\right]$$

with a replica index a. In this technique a physical observable is given by

$$\langle O(\bar{\psi},\psi)\rangle = \lim_{R\to 0}\frac{1}{R}\int \mathcal{D}V\mathcal{D}U\, P[V,U]\int \mathcal{D}\bar{\psi}^a\mathcal{D}\psi^a O(\bar{\psi}^a,\psi^a)$$
$$\times\exp\left[-\sum_{a=1}^R S_0[\bar{\psi}^a,\psi^a] - \sum_{a=1}^R\int d^4x\bar{\psi}^a(x)(\gamma^0 V(\boldsymbol{x})+U(\boldsymbol{x}))\psi^a(x)\right].$$

In this study we take into account static- and Gaussian-distributed disorders, given by

$$P[V,U] = N\exp\left[-\frac{\int d^3\boldsymbol{x}V^2(\boldsymbol{x})}{2\Gamma_V} - \frac{\int d^3\boldsymbol{x}U^2(\boldsymbol{x})}{2\Gamma_U}\right],$$

where N is a normalization factor. It is straightforward to perform the Gaussian integral for disorders, resulting in

$$\langle O(\bar{\psi},\psi)\rangle = \lim_{R\to 0}\frac{1}{R}\sum_{a=1}^R\int \mathcal{D}\bar{\psi}\mathcal{D}\psi\, O(\bar{\psi}^a,\psi^a)\exp\left[-\sum_{a=1}^R S_0[\bar{\psi}^a,\psi^a] - \sum_{b,c=1}^R S_{\rm dis}[\bar{\psi}^b,\psi^b,\bar{\psi}^c,\psi^c]\right],$$

where disorder-driven effective interactions are [Eq. (11)]

$$S_{\rm dis}[\bar{\psi}^b,\psi^b,\bar{\psi}^c,\psi^c] = -\int_0^\beta d\tau\int_0^\beta d\tau'\int d^3\boldsymbol{x}\frac{\Gamma_V}{2}\bar{\psi}^b(\tau,\boldsymbol{x})\gamma^0\psi^b(\tau,\boldsymbol{x})\bar{\psi}^c(\tau',\boldsymbol{x})\gamma^0\psi^c(\tau',\boldsymbol{x})$$
$$-\int_0^\beta d\tau\int_0^\beta d\tau'\int d^3\boldsymbol{x}\frac{\Gamma_U}{2}\bar{\psi}^b(\tau,\boldsymbol{x})\psi^b(\tau,\boldsymbol{x})\bar{\psi}^c(\tau',\boldsymbol{x})\psi^c(\tau',\boldsymbol{x}).$$

2. Renormalized perturbation theory

From now on, we focus on the case of a zero chemical potential. We start from the following effective action

$$S_B = \int d^{d+1}x\bar{\psi}_B^a(x)(\gamma^0\partial_0 + v_{B\imath}\gamma^k\partial_k + c_{B\mu}\gamma^\mu\gamma^5)\psi_B^a(x)$$
$$-\int_0^\beta d\tau\int_0^\beta d\tau'\int d^d\boldsymbol{x}\frac{\Gamma_{BV}}{2}\bar{\psi}_B^b(\tau,\boldsymbol{x})\gamma^0\psi_B^b(\tau,\boldsymbol{x})\bar{\psi}_B^c(\tau',\boldsymbol{x})\gamma^0\psi_B^c(\tau',\boldsymbol{x})$$
$$-\int_0^\beta d\tau\int_0^\beta d\tau'\int d^d\boldsymbol{x}\frac{\Gamma_{BU}}{2}\bar{\psi}_B^b(\tau,\boldsymbol{x})\psi_B^b(\tau,\boldsymbol{x})\bar{\psi}_B^c(\tau',\boldsymbol{x})\psi_B^c(\tau',\boldsymbol{x}),$$

where summations on the replica indices are implied. The subscript B denotes bare, meaning that this effective action is defined at an ultraviolet (UV) scale. Note that we have generalized dimensions to $d+1$ (space + time) for dimensional regularization.

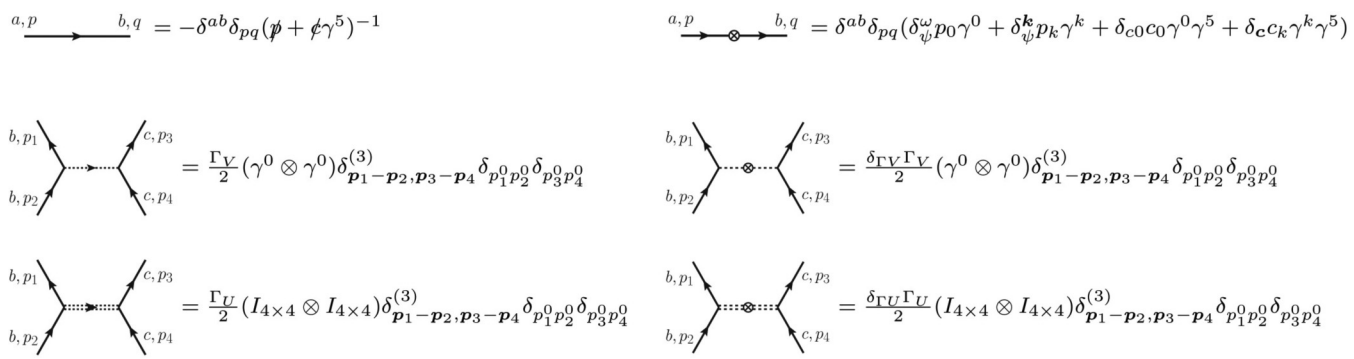

FIG. 6. Feynman rules in the momentum and frequency space. A single-dashed line represents an intravalley scattering while a double-dashed line represents an intervalley scattering.

Performing the dimensional analysis, where space and time coordinates have -1 in mass dimension, we observe

$$\dim[\psi] = \frac{d}{2}, \quad \dim[v] = 0, \quad \dim[c_\mu] = 1, \quad \dim[\Gamma_V] = \dim[\Gamma_U] = 2 - d.$$

In this respect we perform the renormalization group analysis in $d + 1 = 3 + \varepsilon$ dimensions, where ε is a small parameter. In the end of the calculation the dimensions are analytically continued to the physical dimensions ($d + 1 = 4$) by setting $\varepsilon = 1$.

Taking into account quantum corrections, divergences would be generated. They can be absorbed into renormalization constants by redefining fields and parameters. Rewriting the bare action in terms of renormalized fields and couplings, we obtain

$$\begin{aligned} S_B = &\int d^{d+1}x\,\bar\psi^a_R(x)\big(Z^\omega_\psi\gamma^0\partial_0 + Z^{\boldsymbol{k}}_\psi v_R\imath\gamma^k\partial_k + Z_{c0}c_{R0}\gamma^0\gamma^5 + Z_{\boldsymbol{c}}c_{Rk}\gamma^k\gamma^5\big)\psi^a_R(x) \\ &- \int_0^\beta d\tau\int_0^\beta d\tau'\int d^d\boldsymbol{x}\,\frac{Z_{\Gamma V}\Gamma_{RV}}{2}\bar\psi^b_R(\tau,\boldsymbol{x})\gamma^0\psi^b_R(\tau,\boldsymbol{x})\bar\psi^c_R(\tau',\boldsymbol{x})\gamma^0\psi^c_R(\tau',\boldsymbol{x}), \\ &- \int_0^\beta d\tau\int_0^\beta d\tau'\int d^d\boldsymbol{x}\,\frac{Z_{\Gamma U}\Gamma_{RU}}{2}\bar\psi^b_R(\tau,\boldsymbol{x})\psi^b_R(\tau,\boldsymbol{x})\bar\psi^c_R(\tau',\boldsymbol{x})\psi^c_R(\tau',\boldsymbol{x}), \end{aligned}$$

where such renormalized fields and parameters are given by

$$\begin{aligned} &\psi^a_B = \big(Z^\omega_\psi\big)^{\frac{1}{2}}\psi^a_R, \quad v_B = Z^{\boldsymbol{k}}_\psi\big(Z^\omega_\psi\big)^{-1}v_R, \quad c_{B0} = Z_{c0}\big(Z^\omega_\psi\big)^{-1}c_{R0}, \\ &c_{Bk} = Z_{\boldsymbol{c}}\big(Z^\omega_\psi\big)^{-1}c_{Rk}, \quad \Gamma_{BV} = Z_{\Gamma V}\big(Z^\omega_\psi\big)^{-2}\Gamma_{RV}, \quad \Gamma_{BU} = Z_{\Gamma U}\big(Z^\omega_\psi\big)^{-2}\Gamma_{RU}. \end{aligned}$$

It is more elaborate to represent this theory by separating the renormalized part from counter terms that are to absorb divergences in the following way [Eq. (12)],

$$\begin{aligned} S_B &= S_R + S_{CT}, \\ S_R &= \int d^{d+1}x\,\bar\psi^a_R(\gamma^0\partial_0 + v_R\imath\gamma^k\partial_k + c_{R0}\gamma^0\gamma^5 + c_{Rk}\gamma^k\gamma^5)\psi^a_R \\ &\quad - \int d\tau\int d\tau'\int d^d\boldsymbol{x}\,\frac{\Gamma_{RV}}{2}\big(\bar\psi^b_R\gamma^0\psi^b_R\big)_\tau\big(\bar\psi^c_R\gamma^0\psi^c_R\big)_{\tau'} - \int d\tau\int d\tau'\int d^d\boldsymbol{x}\,\frac{\Gamma_{RU}}{2}\big(\bar\psi^b_R\psi^b_R\big)_\tau\big(\bar\psi^c_R\psi^c_R\big)_{\tau'}, \\ S_{CT} &= \int d^{d+1}x\,\bar\psi^a_R\big(\delta^\omega_\psi\gamma^0\partial_0 + \delta^{\boldsymbol{k}}_\psi v_R\imath\gamma^k\partial_k + \delta_{c0}c_{R0}\gamma^0\gamma^5 + \delta_{\boldsymbol{c}}c_{Rk}\gamma^k\gamma^5\big)\psi^a_R \\ &\quad - \int d\tau\int d\tau'\int d^d\boldsymbol{x}\,\frac{\delta_{\Gamma V}\Gamma_{RV}}{2}\big(\bar\psi^b_R\gamma^0\psi^b_R\big)_\tau\big(\bar\psi^c_R\gamma^0\psi^c_R\big)_{\tau'} - \int d\tau\int d\tau'\int d^d\boldsymbol{x}\,\frac{\delta_{\Gamma U}\Gamma_{RU}}{2}\big(\bar\psi^b_R\psi^b_R\big)_\tau\big(\bar\psi^c_R\psi^c_R\big)_{\tau'}, \end{aligned}$$

where $Z^\omega_\psi = 1 + \delta^\omega_\psi$, $Z^{\boldsymbol{k}}_\psi = 1 + \delta^{\boldsymbol{k}}_\psi$, $Z_{c0} = 1 + \delta_{c0}$, $Z_{\boldsymbol{c}} = 1 + \delta_{\boldsymbol{c}}$, $Z_{\Gamma V} = 1 + \delta_{\Gamma V}$, and $Z_{\Gamma U} = 1 + \delta_{\Gamma U}$.

3. Feynman rules

In the momentum and frequency space the effective action is written as

$$S[\bar\psi^a,\psi^a] = \sum_p \bar\psi^a_p(\not{p} + \not{c}\gamma^5)\psi^a_p - \frac{1}{L^3}\sum_{p_j}\left[\frac{\Gamma_V}{2}\big(\bar\psi^b_{p_1}\gamma^0\psi^b_{p_2}\big)\big(\bar\psi^c_{p_3}\gamma^0\psi^c_{p_4}\big) + \frac{\Gamma_U}{2}\big(\bar\psi^b_{p_1}\psi^b_{p_2}\big)\big(\bar\psi^c_{p_3}\psi^c_{p_4}\big)\right]\delta^{(3)}_{\boldsymbol{p}_1-\boldsymbol{p}_2,\boldsymbol{p}_3-\boldsymbol{p}_4}\delta_{p_1^0p_2^0}\delta_{p_3^0p_4^0},$$

where Feynman rules are given in Fig. 6.

Since there is a chiral gauge field in the kinetic-energy part, the free propagator becomes a little bit complex. Considering the following identity

$$(\not{p}+\not{c}\gamma^5)(\not{p}-\not{c}\gamma^5)(p^2+c^2+2p\cdot c\gamma^5)=(p^2+c^2-2p\cdot c\gamma^5)(p^2+c^2+2p\cdot c\gamma^5)=(p+c)^2(p-c)^2,$$

we obtain an electron Green's function

$$G(p)=-(\not{p}+\not{c}\gamma^5)^{-1}=-\frac{(\not{p}-\not{c}\gamma^5)(p^2+c^2+2p\cdot c\gamma^5)}{(p+c)^2(p-c)^2}.$$

We introduce the following expression with a Feynman parameter for the renormalization group analysis

$$G(p)=-\int_0^1 dx\,\frac{(\not{p}-\not{c}\gamma^5)(p^2+c^2+2p\cdot c\gamma^5)}{[(p+(1-2x)c)^2+4x(1-x)c^2]^2}.$$

For a future use, we rearrange it in terms of $\boldsymbol{p}$ as

$$\begin{aligned}
G(p)&=\int_0^1 dx\,\frac{\boldsymbol{p}^2 p_i\gamma^i+\boldsymbol{p}^2(p_0\gamma^0-\not{c}\gamma^5)+p_ip_j(-2c^i\gamma^j\gamma^5)+p_if_1^i(p_0)+f_0(p_0)}{[(\boldsymbol{p}+(1-2x)\boldsymbol{c})^2+\Delta_0(p_0;x)]^2},\\
\Delta_0(p_0;x)&=4x(1-x)\boldsymbol{c}^2-(p_0+c_0)^2+4xp_0c_0,\\
f_1^i(p_0)&=-\gamma^i(p_0\gamma^0-\not{c}\gamma^5)(p_0\gamma^0+\not{c}\gamma^5)+2c^i\gamma^5(p_0\gamma^0-\not{c}\gamma^5),\\
f_0(p_0)&=-(p_0\gamma^0-\not{c}\gamma^5)^2(p_0\gamma^0+\not{c}\gamma^5).
\end{aligned}\tag{B1}$$

Alternatively, we obtain in terms of $\boldsymbol{p}'=\boldsymbol{p}+(1-2x)\boldsymbol{c}$

$$\begin{aligned}
G(p)&=\int_0^1 dx\,\frac{C_3^i\boldsymbol{p}'^2p_i'+C_{2a}\boldsymbol{p}'^2+C_{2b}^{ij}p_i'p_j'+C_1^ip_i'+C_0}{[\boldsymbol{p}'^2+\Delta_0(p_0;x)]^2},\\
C_3^i&=\gamma^i,\quad C_{2a}=\not{u}-\not{c}\gamma^5,\quad C_{2b}^{ij}=-2\gamma^i(u^j+c^j\gamma^5),\\
C_1^i&=-\gamma^i(\not{u}-\not{c}\gamma^5)(\not{u}+\not{c}\gamma^5)-2(u^i-c^i\gamma^5)(\not{u}-\not{c}\gamma^5),\\
C_0&=-(\not{u}-\not{c}\gamma^5)^2(\not{u}+\not{c}\gamma^5),
\end{aligned}\tag{B2}$$

where $u\equiv(p_0,\tilde{\boldsymbol{c}})$ and $\tilde{\boldsymbol{c}}_x\equiv(2x-1)\boldsymbol{c}$. We may use either of these expressions for convenience. Despite their complicated form, they will not be involved much in actual integration procedures.

APPENDIX C: SELF-ENERGY CORRECTIONS

1. Relevant Feynman's diagrams

Within the replica trick, we are allowed to perform the perturbative analysis. The full Green's function of $\mathbf{G}(p,q)=\langle\psi_p\bar{\psi}_q\rangle$ is evaluated up to the Γ^2 order as follows:

$$\begin{aligned}
\mathbf{G}(p,q)&=\lim_{R\to0}\frac{1}{R}\int\mathcal{D}\bar{\psi}\mathcal{D}\psi\left(\psi_p^a\bar{\psi}_q^a\right)e^{-S_0[\bar{\psi}^\alpha,\psi^\alpha]}e^{\frac{1}{L^3}\sum_{p_j}[\frac{\Gamma_V}{2}(\bar{\psi}_{p_1}^b\gamma^0\psi_{p_2}^b)(\bar{\psi}_{p_3}^c\gamma^0\psi_{p_4}^c)+\frac{\Gamma_U}{2}(\bar{\psi}_{p_1}^b\psi_{p_2}^b)(\bar{\psi}_{p_3}^c\psi_{p_4}^c)]\delta^{(3)}_{\boldsymbol{p}_1-\boldsymbol{p}_2,\boldsymbol{p}_3-\boldsymbol{p}_4}\delta_{p_1^0p_2^0}\delta_{p_3^0p_4^0}}\\
&\simeq\lim_{R\to0}\frac{1}{R}\int\mathcal{D}\bar{\psi}\mathcal{D}\psi e^{-S_0[\bar{\psi}^\alpha,\psi^\alpha]}\Bigg[\psi_p^a\bar{\psi}_q^a+\frac{\Gamma_V}{2L^3}\sum_{p_j}\left(\psi_p^a\bar{\psi}_q^a\right)\left(\bar{\psi}_{p_1}^b\gamma^0\psi_{p_2}^b\bar{\psi}_{p_3}^c\gamma^0\psi_{p_4}^c\right)\delta^{(3)}_{\boldsymbol{p}_1-\boldsymbol{p}_2,\boldsymbol{p}_3-\boldsymbol{p}_4}\delta_{p_1^0p_2^0}\delta_{p_3^0p_4^0}\\
&\quad+\frac{\Gamma_U}{2L^3}\sum_{p_j}\left(\psi_p^a\bar{\psi}_q^a\right)\left(\bar{\psi}_{p_1}^b\psi_{p_2}^b\bar{\psi}_{p_3}^c\psi_{p_4}^c\right)\delta^{(3)}_{\boldsymbol{p}_1-\boldsymbol{p}_2,\boldsymbol{p}_3-\boldsymbol{p}_4}\delta_{p_1^0p_2^0}\delta_{p_3^0p_4^0}\\
&\quad+\frac{\Gamma_V^2}{8(L^3)^2}\sum_{p_jp_j'}\left(\psi_p^a\bar{\psi}_q^a\right)\left(\bar{\psi}_{p_1}^b\gamma^0\psi_{p_2}^b\bar{\psi}_{p_3}^c\gamma^0\psi_{p_4}^c\right)\left(\bar{\psi}_{p_1'}^{b'}\gamma^0\psi_{p_2'}^{b'}\bar{\psi}_{p_3'}^{c'}\gamma^0\psi_{p_4'}^{c'}\right)\delta^{(3)}_{\boldsymbol{p}_1-\boldsymbol{p}_2,\boldsymbol{p}_3-\boldsymbol{p}_4}\delta_{p_1^0p_2^0}\delta_{p_3^0p_4^0}\delta^{(3)}_{\boldsymbol{p}_1'-\boldsymbol{p}_2',\boldsymbol{p}_3'-\boldsymbol{p}_4'}\delta_{p_1'^0p_2'^0}\delta_{p_3'^0p_4'^0}\\
&\quad+\frac{\Gamma_U^2}{8(L^3)^2}\sum_{p_jp_j'}\left(\psi_p^a\bar{\psi}_q^a\right)\left(\bar{\psi}_{p_1}^b\psi_{p_2}^b\bar{\psi}_{p_3}^c\psi_{p_4}^c\right)\left(\bar{\psi}_{p_1'}^{b'}\psi_{p_2'}^{b'}\bar{\psi}_{p_3'}^{c'}\psi_{p_4'}^{c'}\right)\delta^{(3)}_{\boldsymbol{p}_1-\boldsymbol{p}_2,\boldsymbol{p}_3-\boldsymbol{p}_4}\delta_{p_1^0p_2^0}\delta_{p_3^0p_4^0}\delta^{(3)}_{\boldsymbol{p}_1'-\boldsymbol{p}_2',\boldsymbol{p}_3'-\boldsymbol{p}_4'}\delta_{p_1'^0p_2'^0}\delta_{p_3'^0p_4'^0}\\
&\quad+\frac{\Gamma_V\Gamma_U}{4(L^3)^2}\sum_{p_jp_j'}\left(\psi_p^a\bar{\psi}_q^a\right)\left(\bar{\psi}_{p_1}^b\gamma^0\psi_{p_2}^b\bar{\psi}_{p_3}^c\gamma^0\psi_{p_4}^c\right)\left(\bar{\psi}_{p_1'}^{b'}\psi_{p_2'}^{b'}\bar{\psi}_{p_3'}^{c'}\psi_{p_4'}^{c'}\right)\delta^{(3)}_{\boldsymbol{p}_1-\boldsymbol{p}_2,\boldsymbol{p}_3-\boldsymbol{p}_4}\delta_{p_1^0p_2^0}\delta_{p_3^0p_4^0}\delta^{(3)}_{\boldsymbol{p}_1'-\boldsymbol{p}_2',\boldsymbol{p}_3'-\boldsymbol{p}_4'}\delta_{p_1'^0p_2'^0}\delta_{p_3'^0p_4'^0}\Bigg],
\end{aligned}$$

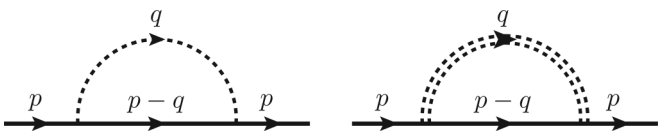

FIG. 7. Self-energy corrections in the first order. There are two Fock diagrams for intravalley and intervalley scattering, respectively.

where summations on the replica indices are implied. Feynman diagrams whose internal lines are not connected to external lines always vanish due to the replica symmetry (all Green's functions with different replica indices are identical) and the replica limit ($\lim_{R\to 0}\frac{1}{R}$). For details, we refer to Ref. [10].

We find self-energy corrections in the first order (Fig. 7),

$$\begin{aligned}\Sigma^{(1)}(p) &= \frac{\Gamma_V}{L^3}\sum_q \gamma^0 G(p-q)\gamma^0\delta_{q^0 0} \\ &\quad + \frac{\Gamma_U}{L^3}\sum_q G(p-q)\delta_{q^0 0} \\ &\equiv \Sigma_V^{(1)}(p) + \Sigma_U^{(1)}(p). \end{aligned} \tag{C1}$$

Likewise, we find self-energy corrections in the second order (Fig. 8).

$$\begin{aligned}\Sigma^{(2),r}(p) &= \frac{\Gamma_V^2}{(L^3)^2}\sum_{q,l}\gamma^0 G(p-q)\gamma^0 G(p-q-l)\gamma^0 G(p-q)\gamma^0\delta_{q^0 0}\delta_{l^0 0} \\ &\quad + \frac{\Gamma_V\Gamma_U}{(L^3)^2}\sum_{q,l}\gamma^0 G(p-q)G(p-q-l)G(p-q)\gamma^0\delta_{q^0 0}\delta_{l^0 0} \\ &\quad + \frac{\Gamma_U\Gamma_V}{(L^3)^2}\sum_{q,l} G(p-q)\gamma^0 G(p-q-l)\gamma^0 G(p-q)\delta_{q^0 0}\delta_{l^0 0} \\ &\quad + \frac{\Gamma_U^2}{(L^3)^2}\sum_{q,l} G(p-q)G(p-q-l)G(p-q)\delta_{q^0 0}\delta_{l^0 0}, \\ &\equiv \Sigma_{VV}^{(2),r}(p) + \Sigma_{VU}^{(2),r}(p) + \Sigma_{UV}^{(2),r}(p) + \Sigma_{UU}^{(2),r}(p) \end{aligned} \tag{C2}$$

$$\begin{aligned}\Sigma^{(2),c}(p) &= \frac{\Gamma_V^2}{(L^3)^2}\sum_{q,l}\gamma^0 G(p-q)\gamma^0 G(p-q-l)\gamma^0 G(p-l)\gamma^0\delta_{q^0 0}\delta_{l^0 0} \\ &\quad + \frac{\Gamma_V\Gamma_U}{(L^3)^2}\sum_{q,l}\gamma^0 G(p-q)G(p-q-l)\gamma^0 G(p-l)\delta_{q^0 0}\delta_{l^0 0} \\ &\quad + \frac{\Gamma_U\Gamma_V}{(L^3)^2}\sum_{q,l}\gamma^0 G(p-q)G(p-q-l)\gamma^0 G(p-l)\delta_{q^0 0}\delta_{l^0 0} \\ &\quad + \frac{\Gamma_U^2}{(L^3)^2}\sum_{q,l} G(p-q)G(p-q-l)G(p-l)\delta_{q^0 0}\delta_{l^0 0} \\ &\equiv \Sigma_{VV}^{(2),c}(p) + \Sigma_{VU}^{(2),c}(p) + \Sigma_{UV}^{(2),c}(p) + \Sigma_{UU}^{(2),c}(p). \end{aligned} \tag{C3}$$

2. Evaluation of relevant diagrams

From now on, we evaluate self-energy diagrams one by one. Since there are two types of interactions, we have many diagrams to evaluate, especially, in the two loop-order. Instead of struggling to evaluate them one by one, we're going to find integration formulas for products of Green's functions and make a use of them for the same types of diagrams.

a. One-loop order: Fock diagrams

First, we evaluate the first-order Fock diagram

$$\Sigma^{(1)}(p) = \Gamma_V\gamma^0 I_1(p)\gamma^0 + \Gamma_U I_1(p),$$

where $I_1(p)$ is given by

$$I_1(p) = \int\frac{d^{d+1}q}{(2\pi)^{d+1}}2\pi\delta(q_0)G(p-q) = \int\frac{d^d\boldsymbol{q}}{(2\pi)^d}G(p_0,\boldsymbol{p}-\boldsymbol{q}) = \int\frac{d^d\boldsymbol{q}}{(2\pi)^d}G(p_0,-\boldsymbol{q}).$$

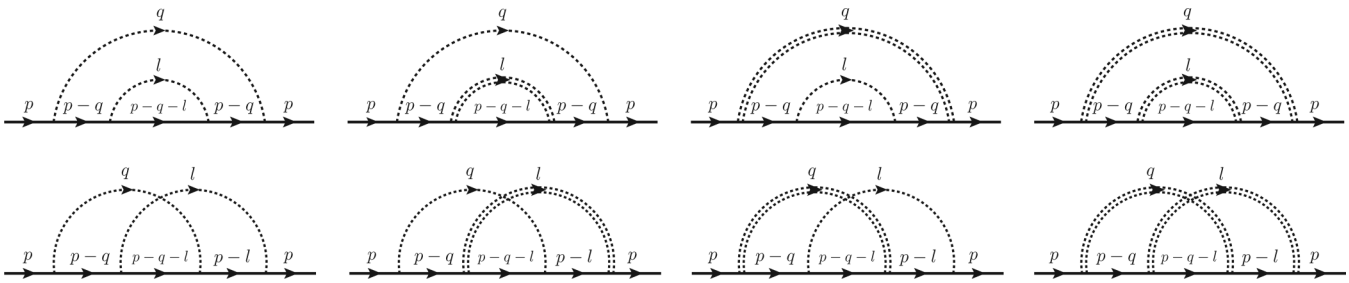

FIG. 8. Self-energy corrections in the second order. There are two distinct types of diagrams, i.e., rainbow diagrams and crossed diagrams. Diagrams in each type are distinguished by interaction vertices (two intravalley scattering, one intravalley and one intervalley scattering, etc.). So, totally there are eight diagrams for the second-order self-energy corrections.

With Eq. (B2), the Green's function is given by

$$G(p_0,-\boldsymbol{q}) = \int_0^1 dx \frac{-C_3^i \boldsymbol{q}'^2 q_i' + C_{2a}\boldsymbol{q}'^2 + C_{2b}^{ij} q_i' q_j' - C_1^i q_i' + C_0}{[\boldsymbol{q}'^2 + \Delta_0(p_0;x)]^2},$$

where $\boldsymbol{q}' = \boldsymbol{q} + \tilde{\boldsymbol{c}}_x$.

Dropping $\boldsymbol{q}'$-odd terms, we have

$$I_1 = \int_0^1 dx \int \frac{d^d\boldsymbol{q}'}{(2\pi)^d} \frac{C_{2a}\boldsymbol{q}'^2 + C_{2b}^{ij} q_i' q_j' + C_0}{[\boldsymbol{q}'^2 + \Delta_0(p_0;x)]^2} = \int_0^1 dx \left[\left(\frac{d}{2} C_{2a} + \frac{1}{2} C_{2b}^{ii} \right) \frac{\Gamma\left(\frac{2-d}{2}\right)}{(4\pi)^{\frac{d}{2}} \Delta_0^{\frac{2-d}{2}}} + \frac{C_0 \Gamma\left(\frac{4-d}{2}\right)}{(4\pi)^{\frac{d}{2}} \Delta_0^{\frac{4-d}{2}}} \right]. \tag{C4}$$

Then, the self-energy is given by

$$\Sigma^{(1)}(p) = \Gamma_V \int_0^1 dx \left[\frac{\left(\frac{d}{2}\bar{C}_{2a} + \frac{1}{2}\bar{C}_{2b}^{ii}\right)\Gamma\left(\frac{2-d}{2}\right)}{(4\pi)^{\frac{d}{2}} \Delta_0^{\frac{2-d}{2}}} + \frac{\bar{C}_0 \Gamma\left(\frac{4-d}{2}\right)}{(4\pi)^{\frac{d}{2}} \Delta_0^{\frac{4-d}{2}}} \right] + \Gamma_U \int_0^1 dx \left[\frac{\left(\frac{d}{2} C_{2a} + \frac{1}{2} C_{2b}^{ii}\right)\Gamma\left(\frac{2-d}{2}\right)}{(4\pi)^{\frac{d}{2}} \Delta_0^{\frac{2-d}{2}}} + \frac{C_0 \Gamma\left(\frac{4-d}{2}\right)}{(4\pi)^{\frac{d}{2}} \Delta_0^{\frac{4-d}{2}}} \right],$$

where we have introduced a bar notation: $\bar{A} \equiv \gamma^0 A \gamma^0$. Since we perform dimensional regularization in $d = 2 + \varepsilon$, the term containing C_0 gives only a finite value. A relevant part for renormalization is

$$\begin{aligned}
\Sigma^{(1)}(p) &\simeq \frac{\Gamma_V}{4\pi} \int_0^1 dx \left[\left(\frac{d}{2}(p_0\gamma^0 - \tilde{c}_{xk}\gamma^k + c_0\gamma^0\gamma^5 - c_k\gamma^k\gamma^5) + \frac{1}{2}(-2\tilde{c}_{xk}\gamma^k + 2c_k\gamma^k\gamma^5) \right) \Gamma\left(\frac{2-d}{2}\right) \left(\frac{\Delta_0}{4\pi}\right)^{\frac{d-2}{2}} \right] \\
&\quad + \frac{\Gamma_U}{4\pi} \int_0^1 dx \left[\left(\frac{d}{2}(p_0\gamma^0 + \tilde{c}_{xk}\gamma^k - c_0\gamma^0\gamma^5 - c_k\gamma^k\gamma^5) + \frac{1}{2}(2\tilde{c}_{xk}\gamma^k + 2c_k\gamma^k\gamma^5) \right) \Gamma\left(\frac{2-d}{2}\right) \left(\frac{\Delta_0}{4\pi}\right)^{\frac{d-2}{2}} \right] \\
&= -\frac{\Gamma_V}{2\pi\varepsilon}(p_0\gamma^0 + c_0\gamma^0\gamma^5) - \frac{\Gamma_U}{2\pi\varepsilon}(p_0\gamma^0 - c_0\gamma^0\gamma^5) + O(1),
\end{aligned} \tag{C5}$$

where $\tilde{c}_{xk}$ terms vanish after the integration over x.

Based on this result, we find propagator counterterms in the following way:

$$-\frac{\Gamma_V}{2\pi\varepsilon}(p_0\gamma^0 + c_0\gamma^0\gamma^5) - \frac{\Gamma_U}{2\pi\varepsilon}(p_0\gamma^0 - c_0\gamma^0\gamma^5) + O(1) + \left(\delta_\psi^\omega p_0\gamma^0 + \delta_\psi^{\boldsymbol{k}} p_k\gamma^k + \delta_{c0}c_0\gamma^0\gamma^5 + \delta_{\boldsymbol{c}}c_k\gamma^k\gamma^5\right) = \text{finite}.$$

As a result, propagator counterterms up to the one-loop level are obtained as

$$\delta_\psi^\omega = \frac{\Gamma_V}{2\pi\varepsilon} + \frac{\Gamma_U}{2\pi\varepsilon}, \quad \delta_\psi^{\boldsymbol{k}} = 0, \quad \delta_{c0} = \frac{\Gamma_V}{2\pi\varepsilon} - \frac{\Gamma_U}{2\pi\varepsilon}, \quad \delta_{\boldsymbol{c}} = 0. \tag{C6}$$

b. Two-loop order I: Rainbow diagrams

Next, we evaluate the rainbow diagrams

$$\begin{aligned}
\Sigma^{(2),r}(p) = \Gamma_V^2 I_{3r}(p)[M_1 = M_2 = \gamma^0] + \Gamma_V\Gamma_U I_{3r}(p)[M_1 = \gamma^0, M_2 = I_{4\times4}] \\
+ \Gamma_U\Gamma_V I_{3r}(p)[M_1 = I_{4\times4}, M_2 = \gamma^0] + \Gamma_U^2 I_{3r}(p)[M_1 = M_2 = I_{4\times4}],
\end{aligned}$$

where I_{3r} is given by

$$I_{3r}(p) = \int \frac{d^{d+1}q}{(2\pi)^{d+1}} 2\pi\delta(q_0) \int \frac{d^{d+1}l}{(2\pi)^{d+1}} 2\pi\delta(l_0) M_1 G(p-q) M_2 G(p-q-l) M_2 G(p-q) M_1.$$

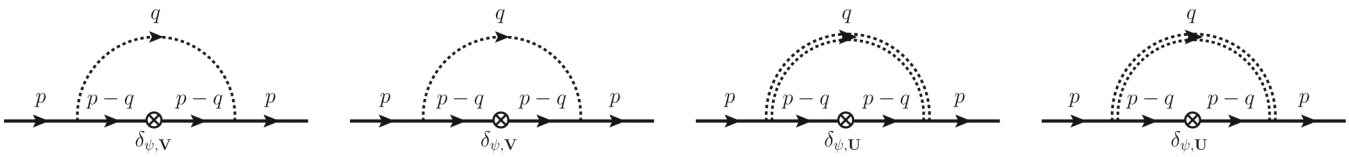

FIG. 9. One-loop self-energy diagrams containing the first-order propagator counterterms given in Eq. (C6). Added to the rainbow diagrams, these contributions cancel the divergent part of I_1 in the rainbow diagrams, leaving only a finite part of I_1 to participate in the remaining calculation.

We may simplify this expression with I_1 as

$$\begin{aligned} I_{3r}(p) &= \int \frac{d^{d+1}q}{(2\pi)^{d+1}} 2\pi\delta(q_0) M_1 G(p-q) M_2 \left[\int \frac{d^{d+1}l}{(2\pi)^{d+1}} 2\pi\delta(l_0) G(p-q-l) \right] M_2 G(p-q) M_1 \\ &= \int \frac{d^d \boldsymbol{q}}{(2\pi)^d} M_1 G(p_0, \boldsymbol{p}-\boldsymbol{q}) M_2 I_1(p-q) M_2 G(p_0, \boldsymbol{p}-\boldsymbol{q}) M_1 \\ &= \int \frac{d^d \boldsymbol{q}}{(2\pi)^d} M_1 G(p_0, -\boldsymbol{q}) M_2 I_1(p_0) M_2 G(p_0, -\boldsymbol{q}) M_1, \end{aligned}$$

where we used $I_1(p_0, -\boldsymbol{q}) = I_1(p_0)$.

Taking into account

$$\frac{1}{((p_0-c_0)^2-(\boldsymbol{q}+\boldsymbol{c}))^2((p_0+c_0)^2-(\boldsymbol{q}-\boldsymbol{c}))^2} = \int_0^1 dy \frac{6y(1-y)}{[\boldsymbol{q}'^2+\Delta_0(p_0;y)]^4}$$

with $\boldsymbol{q}' = \boldsymbol{q} + \tilde{\boldsymbol{c}}_y$ and resorting to the representation of Eq. (B2), we reach the following expression

$$\begin{aligned} I_{3r} = \int_0^1 dy 6y(1-y) \int \frac{d^d \boldsymbol{q}'}{(2\pi)^d} \\ \times \frac{M_1\left(-C_3^i \boldsymbol{q}'^2 q_i' + C_{2a}\boldsymbol{q}'^2 + C_{2b}^{ij} q_i' q_j' - C_1^i q_i' + C_0\right) M_2 I_1 M_2 \left(-C_3^k \boldsymbol{q}'^2 q_k' + C_{2a}\boldsymbol{q}'^2 + C_{2b}^{kl} q_k' q_l' - C_1^k q_k' + C_0\right) M_1}{[\boldsymbol{q}'^2 + \Delta_0(p_0;y)]^4}. \end{aligned}$$

There are many even terms contributing to the integration. However, it turns out that we have to consider the product of C_3^is only. This is because the divergent part of I_1 is canceled by the one-loop self-energy diagrams containing the first-order counterterm, so only the finite part of I_1 participates in the remaining calculation[‡]. In other words, divergences may arise only by the q^6 term in the $\boldsymbol{q}$ integration. For now, we just assume it (we will be back to this point later).

Keeping this term only, we have

$$\begin{aligned} I_{3r}(p) &= \int_0^1 dy 6y(1-y) \int \frac{d^d \boldsymbol{q}}{(2\pi)^d} \frac{(\boldsymbol{q}^2) q_i q_j \left(M_1 C_3^i M_2 I_1 M_2 C_3^j M_1\right)}{[\boldsymbol{q}^2 + \Delta_0(p_0;y)]^4} \\ &= \frac{(d+4)(d+2)\Gamma\left(\frac{2-d}{2}\right)}{8(4\pi)^{\frac{d}{2}}} \int_0^1 dy \frac{y(1-y)}{\Delta_0^{\frac{2-d}{2}}(y)} \left(M_1 C_3^i M_2 I_1 M_2 C_3^i M_1\right). \end{aligned}$$

Then, the second-order self-energy correction for the rainbow diagrams is

$$\Sigma^{(2),r}(p) = \frac{(d+4)(d+2)\Gamma\left(\frac{2-d}{2}\right)}{8(4\pi)^{\frac{d}{2}}} \int_0^1 dy \frac{y(1-y)}{\Delta_0^{\frac{2-d}{2}}(y)} \left[\Gamma_V^2 (\gamma^i I_1 \gamma^i) + 2\Gamma_V \Gamma_U (\gamma^0 \gamma^i I_1 \gamma^i \gamma^0) + \Gamma_U^2 (\gamma^i I_1 \gamma^i)\right].$$

When performing the renormalization group analysis in the second order, we should include consistently one-loop self-energy corrections made of a tree-level vertex and a one-loop propagator counterterm, given by (Fig. 9)

$$\begin{aligned} \Sigma^{(1),\delta_\psi}(p) &= \Gamma_V \int \frac{d^{d+1}q}{(2\pi)^{d+1}} 2\pi\delta(q_0) \gamma^0 G(p-q) \left(\delta_\psi^\omega p_0 \gamma^0 + \delta_\psi^{\boldsymbol{k}} p_k \gamma^k + \delta_{c0} c_0 \gamma^0 \gamma^5 + \delta_{\boldsymbol{c}} c_k \gamma^k \gamma^5\right) G(p-q) \gamma^0 \\ &\quad + \Gamma_U \int \frac{d^{d+1}q}{(2\pi)^{d+1}} 2\pi\delta(q_0) G(p-q) \left(\delta_\psi^\omega p_0 \gamma^0 + \delta_\psi^{\boldsymbol{k}} p_k \gamma^k + \delta_{c0} c_0 \gamma^0 \gamma^5 + \delta_{\boldsymbol{c}} c_k \gamma^k \gamma^5\right) G(p-q) \\ &= \Gamma_V \frac{(d+4)(d+2)\Gamma\left(\frac{2-d}{2}\right)}{8(4\pi)^{\frac{d}{2}}} \int_0^1 dy \frac{y(1-y)}{\Delta_0^{\frac{2-d}{2}}(y)} \gamma^0 \gamma^i [-\Gamma_V \gamma^0 \mathrm{div}(I_1) \gamma^0 - \Gamma_U \mathrm{div}(I_1)] \gamma^i \gamma^0 \end{aligned}$$

$$
\begin{aligned}
&+\Gamma_U\frac{(d+4)(d+2)\Gamma\left(\frac{2-d}{2}\right)}{8(4\pi)^{\frac{d}{2}}}\int_0^1 dy\frac{y(1-y)}{\Delta_0^{\frac{2-d}{2}}(y)}\gamma^i[-\Gamma_V\gamma^0\mathrm{div}(I_1)\gamma^0-\Gamma_U\mathrm{div}(I_1)]\gamma^i\\
&=-\frac{(d+4)(d+2)\Gamma\left(\frac{2-d}{2}\right)}{8(4\pi)^{\frac{d}{2}}}\int_0^1 dy\frac{y(1-y)}{\Delta_0^{\frac{2-d}{2}}(y)}\left[\Gamma_V^2\gamma^i\mathrm{div}(I_1)\gamma^i+2\Gamma_V\Gamma_U\gamma^0\gamma^i\mathrm{div}(I_1)\gamma^i\gamma^0+\Gamma_U^2\gamma^i\mathrm{div}(I_1)\gamma^i\right]\\
&\equiv\Sigma_{VV}^{(1),\delta_\psi}(p)+\Sigma_{VU}^{(1),\delta_\psi}(p)+\Sigma_{UV}^{(1),\delta_\psi}(p)++\Sigma_{UU}^{(1),\delta_\psi}(p),
\end{aligned}
$$

where $\mathrm{div}(\cdots)$ means the divergent part of $(\cdots)$. If we add these to the rainbow diagrams, the divergent part of I_1 in the rainbow diagrams is eliminated and only a finite part participates in the remaining computation (so the remark of ‡ is proved).

Writing it as $\mathrm{fin}(I_1)\equiv I_1-\mathrm{div}(I_1)=\int_0^1 dx\frac{C_0\Gamma(\frac{4-d}{2})}{(4\pi)^{d/2}\Delta_0^{(4-d)/2}}$, we obtain

$$
\Sigma^{(2),r}+\Sigma^{(1),\delta_\psi}=\frac{(d+4)(d+2)\Gamma\left(\frac{2-d}{2}\right)}{8(4\pi)^{\frac{d}{2}}}\int_0^1 dy\frac{y(1-y)}{\Delta_0^{\frac{2-d}{2}}(y)}\left[\Gamma_V^2\gamma^i\mathrm{fin}(I_1)\gamma^i+2\Gamma_V\Gamma_U\gamma^0\gamma^i\mathrm{fin}(I_1)\gamma^i\gamma^0+\Gamma_U^2\gamma^i\mathrm{fin}(I_1)\gamma^i\right].
$$

An expansion about $d=2+\varepsilon$ gives

$$
\frac{(d+4)(d+2)\Gamma(\frac{2-d}{2})}{8(4\pi)^{\frac{d}{2}}}\int_0^1 dy\frac{y(1-y)}{\Delta_0^{\frac{2-d}{2}}(y)}\int_0^1 dx\frac{C_0(x)\Gamma\left(\frac{4-d}{2}\right)}{(4\pi)^{\frac{d}{2}}\Delta_0^{\frac{4-d}{2}}(x)}=-\frac{1}{16\pi^2\varepsilon}\int_0^1 dx\frac{C_0(x)}{\Delta_0(x)}+O(1).
$$

As a result, the relevant part for renormalization is given as

$$
\Sigma^{(2),r}+\Sigma^{(1),\delta_\psi}=-\frac{1}{16\pi^2\varepsilon}\left[\Gamma_V^2\gamma^i\int_0^1 dx\frac{C_0(x)}{\Delta_0(x)}\gamma^i+2\Gamma_V\Gamma_U\gamma^0\gamma^i\int_0^1 dx\frac{C_0(x)}{\Delta_0(x)}\gamma^i\gamma^0+\Gamma_U^2\gamma^i\int_0^1 dx\frac{C_0(x)}{\Delta_0(x)}\gamma^i\right]+O(1).
$$

The remaining calculation is $\int_0^1 dx\frac{C_0(x)}{\Delta_0(x)}$. A straightforward calculation gives

$$
\begin{aligned}
&p_0\gamma^0\left[-1-\frac{\alpha}{2}\ln\left(\frac{\alpha-1}{\alpha+1}\right)-\frac{\beta}{2}\ln\left(\frac{\beta-1}{\beta+1}\right)\right]+c_0\gamma^0\left[\frac{1}{2}\ln\left(\frac{\alpha-1}{\alpha+1}\right)+\frac{1}{2}\ln\left(\frac{\beta-1}{\beta+1}\right)\right]\\
&+c_k\gamma^k\left[-(\alpha+\beta)+\frac{1-\alpha^2}{2}\ln\left(\frac{\alpha-1}{\alpha+1}\right)+\frac{1-\beta^2}{2}\ln\left(\frac{\beta-1}{\beta+1}\right)\right]+c_0\gamma^0\gamma^5\left[1+\frac{\alpha}{2}\ln\left(\frac{\alpha-1}{\alpha+1}\right)+\frac{\beta}{2}\ln\left(\frac{\beta-1}{\beta+1}\right)\right]\\
&+p_0\gamma^0\gamma^5\left[-\frac{1}{2}\ln\left(\frac{\alpha-1}{\alpha+1}\right)-\frac{1}{2}\ln\left(\frac{\beta-1}{\beta+1}\right)\right]+c_k\gamma^k\gamma^5(-1),
\end{aligned}
$$

where $(\alpha,\beta)\equiv ab\pm\sqrt{(a^2-1)(b^2-1)}$ and $a\equiv\frac{p_0}{|\boldsymbol{c}|}$, $b\equiv\frac{c_0}{|\boldsymbol{c}|}$.

Dropping the complex logarithm terms, we have

$$
\begin{aligned}
\gamma^i\int_0^1 dx\frac{C_0(x)}{\Delta_0(x)}\gamma^i&\simeq\gamma^i\left(-p_0\gamma^0-\frac{2p_0c_0}{|\boldsymbol{c}|^2}c_k\gamma^k+c_0\gamma^0\gamma^5-c_k\gamma^k\gamma^5\right)\gamma^i\\
&=-dp_0\gamma^0+(2-d)\frac{2p_0c_0}{|\boldsymbol{c}|^2}c_k\gamma^k-dc_0\gamma^0\gamma^5+(d-2)c_k\gamma^k\gamma^5.
\end{aligned}
$$

As a result, the self-energy correction from rainbow diagrams is

$$
\Sigma^{(2),r}(p)+\Sigma^{(1),\delta_\psi}(p)=\frac{1}{8\pi^2\varepsilon}\left[\Gamma_V^2(p_0\gamma^0+c_0\gamma^0\gamma^5)+\Gamma_U^2(p_0\gamma^0+c_0\gamma^0\gamma^5)+2\Gamma_V\Gamma_U(p_0\gamma^0-c_0\gamma^0\gamma^5)\right]+O(1),\quad\text{(C7)}
$$

where the result is depicted pictorially in Fig. 10.

c. Two-loop order II: Crossed diagrams

Last, we evaluate the crossed diagrams

$$
\begin{aligned}
\Sigma^{(2),c}(p)=&\Gamma_V^2 I_{3c}(p)[M_1=M_2=\gamma^0]+\Gamma_V\Gamma_U I_{3c}(p)[M_1=\gamma^0,M_2=I_{4\times4}]\\
&+\Gamma_U\Gamma_V I_{3c}(p)[M_1=I_{4\times4},M_2=\gamma^0]+\Gamma_U^2 I_{3c}(p)[M_1=M_2=I_{4\times4}],
\end{aligned}
$$

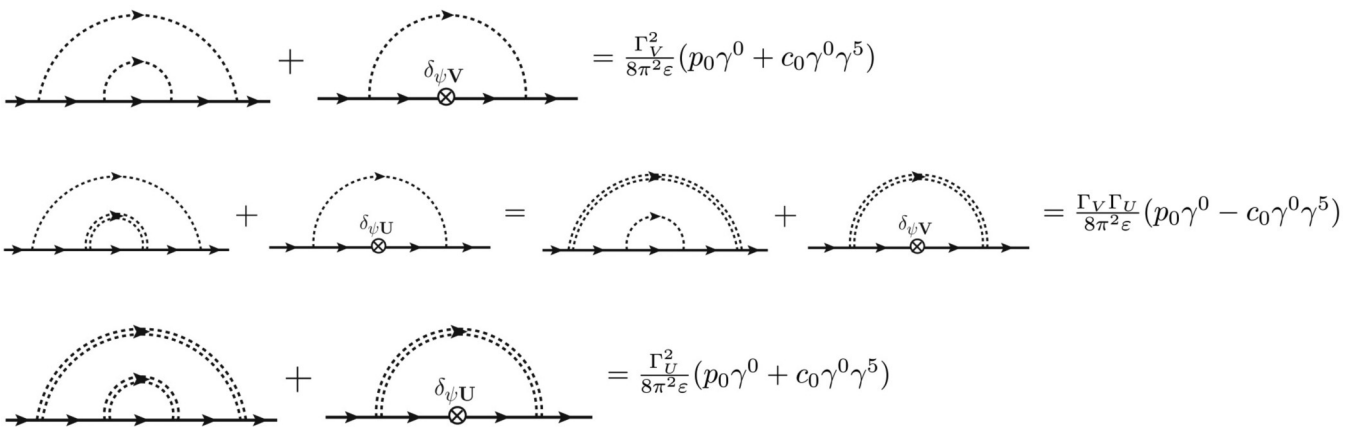

FIG. 10. The result for the rainbow diagrams. Each rainbow diagram is added consistently by one-loop self-energy diagrams made of a tree-level vertex and a one-loop propagator counterterm.

where I_{3c} is given by

$$\begin{aligned} I_{3c}(p) &= \int \frac{d^{d+1}q}{(2\pi)^{d+1}} 2\pi\delta(q_0) \int \frac{d^{d+1}l}{(2\pi)^{d+1}} 2\pi\delta(l_0) M_1 G(p-q) M_2 G(p-q-l) M_1 G(p-l) M_2 \\ &= \int \frac{d^d\boldsymbol{q}}{(2\pi)^d} \int \frac{d^d\boldsymbol{l}}{(2\pi)^d} M_1 G(p_0, \boldsymbol{p}-\boldsymbol{q}) M_2 G(p_0, \boldsymbol{p}-\boldsymbol{q}-\boldsymbol{l}) M_1 G(p_0, \boldsymbol{p}-\boldsymbol{l}) M_2 \\ &= \int \frac{d^d\boldsymbol{q}}{(2\pi)^d} \int \frac{d^d\boldsymbol{l}}{(2\pi)^d} M_1 G(p_0, -\boldsymbol{q}) M_2 G(p_0, -\boldsymbol{q}-\boldsymbol{l}) M_1 G(p_0, -\boldsymbol{l}+\boldsymbol{p}) M_2. \end{aligned}$$

In this case the loop momenta of $\boldsymbol{l}$ and $\boldsymbol{q}$ are interwoven and this makes the analysis more complicated.

First, we perform the integration on $\boldsymbol{q}$. Using Eq. (B2), we have

$$\begin{aligned} &\int_0^1 dx \int_0^1 dy \int \frac{d^d\boldsymbol{q}}{(2\pi)^d} \frac{-C_3^i \boldsymbol{q}'^2 q_i + C_{2a}\boldsymbol{q}'^2 + C_{2b}^{ij} q_i' q_j' - C_1^i q_i' + C_0}{[\boldsymbol{q}'^2 + \Delta_0(p_0; x)]^2} \\ &\quad \times M_2 \frac{-C_3^k (\boldsymbol{q}'+\boldsymbol{l})^2 (q_k'+l_k) + C_{2a}(\boldsymbol{q}'+\boldsymbol{l})^2 + C_{2b}^{kl}(q_k'+l_k)(q_l'+l_l) - C_1^l(q_l'+l_l) + C_0}{[(\boldsymbol{q}'+\boldsymbol{l})^2 + \Delta_0(p_0; y)]^2}. \end{aligned}$$

Denominators are combined as

$$\frac{1}{[\boldsymbol{q}'^2 + \Delta_0(p_0;x)]^2[(\boldsymbol{q}'+\boldsymbol{l})^2 + \Delta_0(p_0;y)]^2} = \int_0^1 dz \frac{6z(1-z)}{[(\boldsymbol{q}'+z\boldsymbol{l})^2 + \Delta_1(p_0, \boldsymbol{l}; x, y, z)]^4},$$

where $\Delta_1 = z(1-z)\boldsymbol{l}^2 + (1-z)\Delta_0(p_0;x) + z\Delta_0(p_0;y)$. Shifting $\boldsymbol{q}' \to \boldsymbol{q}' - z\boldsymbol{l}$ and renaming $\boldsymbol{q}'$ as $\boldsymbol{q}$, we have

$$\begin{aligned} &\int_0^1 dx \int_0^1 dy \int_0^1 dz \int \frac{d^d\boldsymbol{q}}{(2\pi)^d} \frac{6z(1-z)}{[\boldsymbol{q}^2 + \Delta_1]^4} \big(-C_3^i(\boldsymbol{q}-z\boldsymbol{l})^2(q_i - zl_i) \\ &\quad + C_{2a}(\boldsymbol{q}-z\boldsymbol{l})^2 + C_{2b}^{ij}(q_i - zl_i)(q_j - zl_j) - C_1^i(q_i - zl_i) + C_0\big) M_2 \big(-C_3^k(\boldsymbol{q} + (1-z)\boldsymbol{l})^2(q_k + (1-z)l_k) \\ &\quad + C_{2a}(\boldsymbol{q} + (1-z)\boldsymbol{l})^2 + C_{2b}^{kl}(q_k + (1-z)l_k)(q_l + (1-z)l_l) - C_1^k(q_k + (1-z)l_k) + C_0\big). \end{aligned}$$

Despite this complex expression, we need to consider only a few terms for renormalization. This can be understood, considering a simple integral

$$\int \frac{d^d\boldsymbol{q}}{(2\pi)^d} \frac{(\boldsymbol{q}^2)^m}{[\boldsymbol{q}^2 + \Delta]^4} = \frac{\Gamma\left(\frac{8-d-2m}{2}\right)\Gamma\left(\frac{d}{2}+m\right)}{(4\pi)^{\frac{d}{2}}\Gamma\left(\frac{d}{2}\right)\Gamma(4)\Delta^{\frac{8-d-2m}{2}}}. \tag{C8}$$

Since we resort to the dimensional regularization in $d = 2 + \varepsilon$, an integral for m smaller than 3 gives a finite value, and it doesn't participate in renormalization. The product of the q^3 terms (i.e., q^6 term) certainly gives renormalization effects. Other than the q^6 term, even terms of q^4l^2, q^2l^4, and l^6 possibly contribute to renormalization after the $\boldsymbol{l}$ integral because there will be an equal number of momentum l in the denominator and numerator (considering the dimension of an integrand, this fact may be easily estimated, because any dimensionful constant in numerator lowers the superficial degree of divergence of the integral). All of

those come from the product of the C_3 terms, so the relevant part is

$$\int_0^1 dx \int_0^1 dy \int_0^1 dz 6z(1-z) \int \frac{d^d\boldsymbol{q}}{(2\pi)^d} \frac{(\boldsymbol{q}-z\boldsymbol{l})^2(\boldsymbol{q}-z\boldsymbol{l})M_2(\boldsymbol{q}+(1-z)\boldsymbol{l})^2(\boldsymbol{q}+(1-z)\boldsymbol{l})}{[\boldsymbol{q}^2+\Delta_1(p_0,\boldsymbol{l};x,y,z)]^4},$$

where $\boldsymbol{q} \equiv q_i\gamma^i (i=1,2,3)$.

The numerator is arranged as

$$\begin{aligned} N &= (-1)^{1+\frac{1}{4}\mathrm{tr}[M_2]} M_2(\boldsymbol{q}-z\boldsymbol{l})^2(\boldsymbol{q}+(1-z)\boldsymbol{l})^2(\boldsymbol{q}-z\boldsymbol{l})(\boldsymbol{q}+(1-z)\boldsymbol{l}) \\ &= (-1)^{\frac{1}{4}\mathrm{tr}[M_2]} M_2\big[D_6(\boldsymbol{q}^2)^3 + D_{4a}(\boldsymbol{q}^2)^2 + D_{4b}^{ij}\boldsymbol{q}^2 q_i q_j + D_{2a}\boldsymbol{q}^2 + D_{2b}^{ij} q_i q_j + D_0\big] + (\text{odd terms}), \end{aligned}$$

where the coefficients are given by

$$\begin{aligned} &D_6 = 1, \quad D_{4a} = (3z^2-3z+1)\boldsymbol{l}^2, \quad D_{4b}^{ij} = (12z^2-8z)l^i l^j + (2-4z)l^i\gamma^j\boldsymbol{l}, \quad D_{2a} = (3z^4-6z^3+4z^2-z)(\boldsymbol{l}^2)^2, \\ &D_{2b}^{ij} = (12z^4-20z^3+8z^2)\boldsymbol{l}^2 l^i l^j + (-4z^3+6z^2-2z)\boldsymbol{l}^2 l^i\gamma^j\boldsymbol{l}, \quad D_0 = z^3(z-1)^3(\boldsymbol{l}^2)^3. \end{aligned}$$

Now, the integral is easily performed to be

$$\begin{aligned} &\int \frac{d^d\boldsymbol{q}}{(2\pi)^d} \frac{(-1)^{\frac{1}{4}\mathrm{tr}[M_2]} M_2\big[D_6(\boldsymbol{q}^2)^3 + D_{4a}(\boldsymbol{q}^2)^2 + D_{4b}^{ij}\boldsymbol{q}^2 q_i q_j + D_{2a}\boldsymbol{q}^2 + D_{2b}^{ij} q_i q_j + D_0\big]}{[\boldsymbol{q}^2+\Delta_1(\boldsymbol{l};x,y,z)]^4} \\ &= \frac{(-1)^{\frac{1}{4}\mathrm{tr}[M_2]} M_2}{(4\pi)^{\frac{d}{2}}} \left[\frac{d(d+4)(d+2)\Gamma\left(\frac{2-d}{2}\right)}{8\Gamma(4)} \frac{D_6}{\Delta_1^{\frac{2-d}{2}}} + \frac{d(d+2)\Gamma\left(\frac{4-d}{2}\right)}{4\Gamma(4)} \frac{D_{4a}+\frac{D_{4b}^{ii}}{d}}{\Delta_1^{\frac{4-d}{2}}} + \frac{d\Gamma\left(\frac{6-d}{2}\right)}{2\Gamma(4)} \frac{D_{2a}+\frac{D_{2b}^{ii}}{d}}{\Delta_1^{\frac{6-d}{2}}} + \frac{\Gamma\left(\frac{8-d}{2}\right)}{\Gamma(4)} \frac{D_0}{\Delta_1^{\frac{8-d}{2}}} \right]. \end{aligned}$$

Next, we perform the $\boldsymbol{l}$ integral. Using $M_1 M_2 M_1 = M_2$ (since the matrices of M_1 and M_2 are either $I_{4\times4}$ or γ^0), we have

$$\begin{aligned} I_{3c}(p) = \frac{(-1)^{\frac{1}{4}\mathrm{tr}[M_2]}}{(4\pi)^{\frac{d}{2}}} \int_0^1 dx \int_0^1 dy \int_0^1 dz z(1-z) \int \frac{d^d\boldsymbol{l}}{(2\pi)^d} \Bigg[&\frac{d(d+4)(d+2)\Gamma\left(\frac{2-d}{2}\right)}{8} \frac{D_6}{\Delta_1^{\frac{2-d}{2}}} \\ &+ \frac{d(d+2)\Gamma\left(\frac{4-d}{2}\right)}{4} \frac{D_{4a}+\frac{D_{4b}^{ii}}{d}}{\Delta_1^{\frac{4-d}{2}}} + \frac{d\Gamma\left(\frac{6-d}{2}\right)}{2} \frac{D_{2a}+\frac{D_{2b}^{ii}}{d}}{\Delta_1^{\frac{6-d}{2}}} + \frac{\Gamma\left(\frac{8-d}{2}\right)D_0}{\Delta_1^{\frac{8-d}{2}}} \Bigg] M_2 G(p_0,-\boldsymbol{l}+\boldsymbol{p}) M_2 + (\text{finite parts}). \end{aligned}$$

Taking out $z(1-z)$ from $\Delta_1 = z(1-z)\boldsymbol{l}^2 + (1-z)\Delta_0(x) + z\Delta_0(y)$ first, we find that the remaining integrals are such a simple form:

$$\begin{aligned} &\int_0^1 dv \int \frac{d^d\boldsymbol{l}}{(2\pi)^d} \frac{(\boldsymbol{l}^2)^n}{\left[\boldsymbol{l}^2 + \frac{1}{z}\Delta_0(p_0;x) + \frac{1}{1-z}\Delta_0(p_0;y)\right]^{n+\frac{2-d}{2}}} \\ &\times \frac{-(\boldsymbol{l}-\boldsymbol{p})^2(l_i-p_i)\gamma^i + (\boldsymbol{l}-\boldsymbol{p})^2(p_0\gamma^0 - \not{p}\gamma^5) + (l_i-p_i)(l_j-p_j)(-2c^i\gamma^j\gamma^5) - (l_i-p_i)f_1^i(p_0) + f_0(p_0)}{[(\boldsymbol{l}-\boldsymbol{p}+\tilde{\boldsymbol{c}}_v)^2 + \Delta_0(p_0;v)]^2}, \end{aligned}$$

where the cases of $n=0,1,2,3$ correspond to integrals for D_6, D_4, D_2, and D_0, respectively. Such integrations result in $\Gamma(n + \frac{2-d}{2} + 2 - \frac{d}{2} - n - m) = \Gamma(3-d-m)$, where $m=1$ stands for l^2 (the leading even term) and $m=0$ for a constant term in the propagator. Within the dimensional regularization in $d = 2+\varepsilon$, only the integral of $m=1$ possibly gives a divergent factor of $\Gamma(2-d)$. However, in the $n=0$ case we already have $\Gamma(\frac{2-d}{2})$, and we need to consider the constant ($m=0$) term, which turns out to be important. We first compute this term.

The denominator is transformed as

$$\int_0^1 dv \frac{1}{\left[\boldsymbol{l}^2 + \frac{\Delta_0(x)}{z} + \frac{\Delta_0(y)}{1-z}\right]^{\frac{2-d}{2}} [(\boldsymbol{l}-\boldsymbol{p}+\tilde{\boldsymbol{c}}_v)^2 + \Delta_0(v)]^2} = \int_0^1 dv \int_0^1 dw \frac{w(1-w)^{-\frac{d}{2}}\Gamma\left(\frac{6-d}{2}\right)/\Gamma\left(\frac{2-d}{2}\right)}{[(\boldsymbol{l}-w(\boldsymbol{p}-\tilde{\boldsymbol{c}}_v))^2 + \Delta_2(\boldsymbol{p};x,y,z,v,w)]^{\frac{6-d}{2}}},$$

where $\Delta_2 = w(1-w)(\boldsymbol{p}-\tilde{\boldsymbol{c}}_v)^2 + \frac{1-w}{z}\Delta_0(x) + \frac{1-w}{1-z}\Delta_0(y) + w\Delta_0(v)$. This suggests that we may use Eq. (B2) with a slight change. Then, the integral for $m=0$ is

$$\frac{\Gamma\left(\frac{6-d}{2}\right)}{\Gamma\left(\frac{2-d}{2}\right)} \int_0^1 dv \int_0^1 dw w(1-w)^{-\frac{d}{2}} \int \frac{d^d\boldsymbol{l}'}{(2\pi)^d} \frac{C_0(w,v)}{[\boldsymbol{l}'^2 + \Delta_2(w,v)]^{\frac{6-d}{2}}} = \frac{\Gamma(3-d)}{(4\pi)^{\frac{d}{2}}\Gamma\left(\frac{2-d}{2}\right)} \int_0^1 dv \int_0^1 dw w(1-w)^{-\frac{d}{2}} \frac{C_0(w,v)}{\Delta_2(w,v)},$$

where $C_0(w,v)$ is same with that of Eq. (B2) except for $u = [p_0, (1-w)\boldsymbol{p} + w\tilde{\boldsymbol{c}}_v]$. Note $C_0(w=1,v) = C_0(v)$ (the original definition of C_0) and $\Delta_2(w=1,v) = \Delta_0(v)$.

This implies that we may take out a relevant part in the following way

$$\frac{\Gamma(3-d)}{(4\pi)^{\frac{d}{2}}\Gamma\left(\frac{2-d}{2}\right)}\int_0^1 dv\int_0^1 dw w(1-w)^{-\frac{d}{2}}\left[\frac{C_0(v)}{\Delta_0(v)}+\frac{d}{dw}\frac{C_0(w,v)}{\Delta_2(w,v)}\bigg|_{w=1}(w-1)+O(w-1)^2\right]$$
$$=\frac{\Gamma(3-d)}{(4\pi)^{\frac{d}{2}}\Gamma\left(\frac{6-d}{2}\right)}\int_0^1 dv\frac{C_0(v)}{\Delta_0(v)}-\frac{\frac{4\Gamma(3-d)}{(6-d)(4-d)}}{(4\pi)^{\frac{d}{2}}\Gamma\left(\frac{2-d}{2}\right)}\int_0^1 dv\frac{d}{dw}\frac{C_0(w,v)}{\Delta_2(w,v)}\bigg|_{w=1}+\cdots.$$

Note that $\Gamma(\frac{2-d}{2})$ in the first term is canceled after the w integral, but $\Gamma(\frac{2-d}{2})$ in the second term is not. Together with $\Gamma(\frac{2-d}{2})$ originating from the $\boldsymbol{q}$ integral, the first term contributes to a divergent part while the other higher-order terms give only finite values. In short, the above analysis suggests that we should include $\int_0^1 dv\frac{C_0(v)}{\Delta_0(v)}$.

Now, we focus on the $m=1$ case. Since l^2 may arise from l^2 (surely) and l^3 (after momentum shift), we keep them. After the similar analysis as the above, we obtain

$$\int_0^1 dv\int\frac{d^d\boldsymbol{l}}{(2\pi)^d}\frac{(\boldsymbol{l}^2)^n}{\left[\boldsymbol{l}^2+\frac{1}{z}\Delta_0(x)+\frac{1}{1-z}\Delta_0(y)\right]^{n+\frac{2-d}{2}}}\frac{\boldsymbol{l}^2(\not{p}-\not{\epsilon}\gamma^5)-\boldsymbol{l}^2 l_i\gamma^i+l_il_j(-2p^i\gamma^j-2c^i\gamma^j\gamma^5)}{[(\boldsymbol{l}-\boldsymbol{p}+\tilde{\boldsymbol{c}}_v)^2+\Delta_0(p_0;v)]^2}$$
$$=\int_0^1 dv\int_0^1 dw\frac{w(1-w)^{n-\frac{d}{2}}\Gamma\left(n+\frac{6-d}{2}\right)}{\Gamma(2)\Gamma\left(n+\frac{2-d}{2}\right)}\int\frac{d^d\boldsymbol{l}}{(2\pi)^d}\frac{(\boldsymbol{l}^2)^n[\boldsymbol{l}^2(\not{p}-\not{\epsilon}\gamma^5)-\boldsymbol{l}^2 l_i\gamma^i+l_il_j(-2p^i\gamma^j-2c^i\gamma^j\gamma^5)]}{[(\boldsymbol{l}-w(\boldsymbol{p}-\tilde{\boldsymbol{c}}_v))^2+\Delta_2(\boldsymbol{p};x,y,z,v,w)]^{n+\frac{6-d}{2}}}$$
$$\simeq\frac{\Gamma\left(n+\frac{6-d}{2}\right)}{\Gamma\left(n+\frac{2-d}{2}\right)}\int_0^1 dv\int_0^1 dw w(1-w)^{n-\frac{d}{2}}$$
$$\times\int\frac{d^d\boldsymbol{l}}{(2\pi)^d}\frac{(\boldsymbol{l}^2)^n\left[\boldsymbol{l}^2(\not{p}-\not{\epsilon}\gamma^5-w(p_i-\tilde{c}_{vi})\gamma^i)+l_il_j\left(2(n+1)w\left(p^i-\tilde{c}_v^i\right)\gamma^j-2p^i\gamma^j-2c^i\gamma^j\gamma^5\right)\right]}{[\boldsymbol{l}^2+\Delta_2(\boldsymbol{p};x,y,z,v,w)]^{n+\frac{6-d}{2}}},$$

where we have shifted $\boldsymbol{l}\to\boldsymbol{l}+w(\boldsymbol{p}-\tilde{\boldsymbol{c}}_v)$ and kept only the leading even terms including shifted contributions from $(\boldsymbol{l}^2)^n$ and $\boldsymbol{l}^2 l_i$.

After the $\boldsymbol{l}$ integration, we reach the following expression

$$\frac{\Gamma(2-d)\Gamma\left(\frac{d}{2}+n+1\right)}{(4\pi)^{\frac{d}{2}}\Gamma\left(\frac{d}{2}\right)\Gamma\left(n+\frac{2-d}{2}\right)}\int_0^1 dv\int_0^1 dw w(1-w)^{n-\frac{d}{2}}\Delta_2^{d-2}$$
$$\times\left(\not{p}-\not{\epsilon}\gamma^5-w(p_i-\tilde{c}_{vi})\gamma^i+\frac{1}{d}(-2(n+1)w(p_i-\tilde{c}_{vi})\gamma^i+2p_i\gamma^i+2c_i\gamma^i\gamma^5)\right).$$

Considering $d=2+\varepsilon$, Δ_2^{d-2} is not involved in the w and the v integral. The effect of the v integral is just to remove $\tilde{c}_{vi}$. The w integral gives

$$\frac{\Gamma(2-d)}{(4\pi)^{\frac{d}{2}}\Gamma\left(\frac{d}{2}\right)}\frac{\Gamma\left(\frac{d}{2}+n+1\right)}{\Gamma\left(n+\frac{6-d}{2}\right)}\left(\not{p}-\not{\epsilon}\gamma^5+\frac{2}{d}(p_i\gamma^i+c_i\gamma^i\gamma^5)-\frac{2}{n+\frac{6-d}{2}}\frac{2(n+1)+d}{d}p_i\gamma^i\right),$$

where $2/(n+\frac{6-d}{2})$ makes up for the difference due to additional w. Among the remaining Feynman parameters of x,y, and z, only z is effective since there are polynomials of z in the Ds.

The z integrals for each n are performed as (from the first line, $n=0,1,2,3$)

$$\int_0^1 dz\frac{z(1-z)}{z^{\frac{2-d}{2}}(1-z)^{\frac{2-d}{2}}}=\frac{\left[\Gamma\left(\frac{d+2}{2}\right)\right]^2}{\Gamma(d+2)},$$
$$\int_0^1 dzz(1-z)\frac{1-3z(1-z)+\frac{2-12z(1-z)}{d}}{z^{\frac{4-d}{2}}(1-z)^{\frac{4-d}{2}}}=\frac{d^2+8}{d^2}\frac{\left[\Gamma\left(\frac{d+2}{2}\right)\right]^2}{\Gamma(d+2)},$$
$$\int_0^1 dzz(1-z)\frac{z(1-z)\left(-1+3z(1-z)+\frac{-2+12z(1-z)}{d}\right)}{z^{\frac{6-d}{2}}(1-z)^{\frac{6-d}{2}}}=-\frac{d^2+8}{d^2}\frac{\left[\Gamma\left(\frac{d+2}{2}\right)\right]^2}{\Gamma(d+2)},$$
$$\int_0^1 dzz(1-z)\frac{-z^3(1-z)^3}{z^{\frac{8-d}{2}}(1-z)^{\frac{8-d}{2}}}=-\frac{\left[\Gamma\left(\frac{d+2}{2}\right)\right]^2}{\Gamma(d+2)}.$$

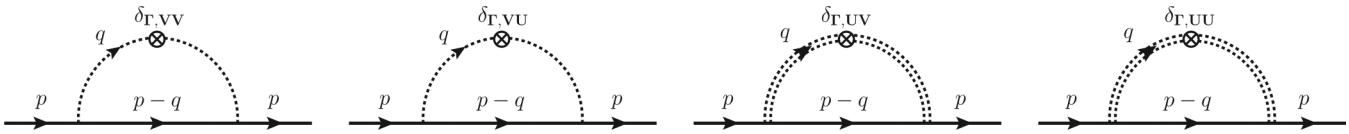

FIG. 11. One-loop self-energy diagrams containing a vertex counterterm. Added to the crossed diagrams, these contributions cancel non-local divergences, arising in the crossed diagrams and leaving local divergences only.

As a result, we obtain

$$
\begin{aligned}
I_{3c}(p) = {} & \frac{\Gamma\left(\frac{2-d}{2}\right)\Gamma(2-d)}{(4\pi)^d\Gamma\left(\frac{d}{2}\right)}\frac{\left[\Gamma\left(\frac{d+2}{2}\right)\right]^2}{\Gamma(d+2)}\Bigg[(-1)^{\frac{1}{4}\mathrm{tr}[M_2]}M_2\left(\not{p}-\not{c}\gamma^5+\frac{2}{d}(p_k\gamma^k+c_k\gamma^k\gamma^5)\right)M_2 \\
& \times\left(\frac{(d+4)(d+2)d}{8}\frac{\Gamma\left(\frac{d+2}{2}\right)}{\Gamma\left(\frac{6-d}{2}\right)}+\frac{(d+2)d(2-d)}{8}\frac{\Gamma\left(\frac{d+2}{2}+1\right)}{\Gamma\left(\frac{6-d}{2}+1\right)}\frac{d^2+8}{d^2}\right. \\
& \left.-\frac{d(4-d)(2-d)}{8}\frac{\Gamma\left(\frac{d+2}{2}+2\right)}{\Gamma\left(\frac{6-d}{2}+2\right)}\frac{d^2+8}{d^2}-\frac{(6-d)(4-d)(2-d)}{8}\frac{\Gamma\left(\frac{d+2}{2}+3\right)}{\Gamma\left(\frac{6-d}{2}+3\right)}\right) \\
& -\frac{2}{d}(-1)^{\frac{1}{4}\mathrm{tr}[M_2]}M_2(p_k\gamma^k)M_2\left(\frac{(d+4)(d+2)d}{8}\frac{2+d}{\frac{6-d}{2}}\frac{\Gamma\left(\frac{d+2}{2}\right)}{\Gamma\left(\frac{6-d}{2}\right)}+\frac{(d+2)d(2-d)}{8}\frac{4+d}{\frac{6-d}{2}+1}\frac{\Gamma\left(\frac{d+2}{2}+1\right)}{\Gamma\left(\frac{6-d}{2}+1\right)}\frac{d^2+8}{d^2}\right. \\
& \left.-\frac{d(4-d)(2-d)}{8}\frac{6+d}{\frac{6-d}{2}+2}\frac{\Gamma\left(\frac{d+2}{2}+2\right)}{\Gamma\left(\frac{6-d}{2}+2\right)}\frac{d^2+8}{d^2}-\frac{(6-d)(4-d)(2-d)}{8}\frac{8+d}{\frac{6-d}{2}+3}\frac{\Gamma\left(\frac{d+2}{2}+3\right)}{\Gamma\left(\frac{6-d}{2}+3\right)}\right)\Bigg] \\
& +\frac{\Gamma\left(\frac{2-d}{2}\right)\Gamma(3-d)}{(4\pi)^d\Gamma\left(\frac{6-d}{2}\right)}\frac{\left[\Gamma\left(\frac{d+2}{2}\right)\right]^2}{\Gamma(d+2)}\frac{(d+4)(d+2)d}{8}(-1)^{\frac{1}{4}\mathrm{tr}[M_2]}M_2\left[\int_0^1 dv\frac{C_0(v)}{\Delta_0(v)}\right]M_2 \\
= {} & \left(\frac{1}{8\pi^2\varepsilon^2}+\frac{5+6\gamma-6\ln 4\pi}{8\pi^2\varepsilon}\right)(-1)^{\frac{1}{4}\mathrm{tr}[M_2]}(p_0\gamma^0)+\frac{1}{16\pi^2\varepsilon}(p_k\gamma^k)+\left(\frac{1}{8\pi^2\varepsilon^2}+\frac{5+6\gamma-6\ln 4\pi}{8\pi^2\varepsilon}\right)(c_0\gamma^0\gamma^5) \\
& -\frac{1}{16\pi^2\varepsilon}(-1)^{\frac{1}{4}\mathrm{tr}[M_2]}(c_k\gamma^k\gamma^5)-\frac{1}{8\pi^2\varepsilon}(-1)^{\frac{1}{4}\mathrm{tr}[M_2]}M_2\left[\int_0^1 dv\frac{C_0(v)}{\Delta_0(v)}\right]M_2+O(1),
\end{aligned}
$$

where we have used the matrix identities:

$$
\begin{aligned}
&(-1)^{\frac{1}{4}\mathrm{tr}[M_2]}M_2\gamma^0M_2=(-1)^{\frac{1}{4}\mathrm{tr}[M_2]}\gamma^0,\quad (-1)^{\frac{1}{4}\mathrm{tr}[M_2]}M_2\gamma^0\gamma^5M_2=-\gamma^0\gamma^5,\\
&(-1)^{\frac{1}{4}\mathrm{tr}[M_2]}M_2\gamma^kM_2=-\gamma^k,\quad (-1)^{\frac{1}{4}\mathrm{tr}[M_2]}M_2\gamma^k\gamma^5M_2=(-1)^{\frac{1}{4}\mathrm{tr}[M_2]}\gamma^k\gamma^5.
\end{aligned}
$$

Finally, the self-energy correction from the crossed diagrams is

$$
\begin{aligned}
\Sigma^{(2),c}(p)= {} & \Gamma_V^2\left[\left(\frac{1}{8\pi^2\varepsilon^2}+\frac{5+6\gamma-6\ln 4\pi}{48\pi^2\varepsilon}\right)(p_0\gamma^0+c_0\gamma^0\gamma^5)+\frac{1}{16\pi^2\varepsilon}p_k\gamma^k-\frac{1}{16\pi^2\varepsilon}c_k\gamma^k\gamma^5-\frac{1}{8\pi^2\varepsilon}\int_0^1 dv\frac{\bar{C}_0(v)}{\Delta_0(v)}\right] \\
& +\Gamma_V\Gamma_U\left[\left(\frac{1}{8\pi^2\varepsilon^2}+\frac{5+6\gamma-6\ln 4\pi}{48\pi^2\varepsilon}\right)(-p_0\gamma^0+c_0\gamma^0\gamma^5)+\frac{1}{16\pi^2\varepsilon}p_k\gamma^k+\frac{1}{16\pi^2\varepsilon}c_k\gamma^k\gamma^5+\frac{1}{8\pi^2\varepsilon}\int_0^1 dv\frac{C_0(v)}{\Delta_0(v)}\right] \\
& +\Gamma_U\Gamma_V\left[\left(\frac{1}{8\pi^2\varepsilon^2}+\frac{5+6\gamma-6\ln 4\pi}{48\pi^2\varepsilon}\right)(p_0\gamma^0+c_0\gamma^0\gamma^5)+\frac{1}{16\pi^2\varepsilon}p_k\gamma^k-\frac{1}{16\pi^2\varepsilon}c_k\gamma^k\gamma^5-\frac{1}{8\pi^2\varepsilon}\int_0^1 dv\frac{\bar{C}_0(v)}{\Delta_0(v)}\right] \\
& +\Gamma_U^2\left[\left(\frac{1}{8\pi^2\varepsilon^2}+\frac{5+6\gamma-6\ln 4\pi}{48\pi^2\varepsilon}\right)(-p_0\gamma^0+c_0\gamma^0\gamma^5)+\frac{1}{16\pi^2\varepsilon}p_k\gamma^k+\frac{1}{16\pi^2\varepsilon}c_k\gamma^k\gamma^5+\frac{1}{8\pi^2\varepsilon}\int_0^1 dv\frac{C_0(v)}{\Delta_0(v)}\right] \\
& +O(1).
\end{aligned}
$$

When we take into account the vertex renormalization, we should introduce consistently self-energy corrections made of a vertex counterterm, given by (Fig. 11)

$$
\Sigma^{(1),\delta_\Gamma}(p)=\delta_{\Gamma V}\Gamma_V\gamma^0I_1(p)\gamma^0+\delta_{\Gamma U}\Gamma_UI_1(p)\equiv\Sigma_{VV}^{(1),\delta_\Gamma}(p)+\Sigma_{VU}^{(1),\delta_\Gamma}(p)+\Sigma_{UV}^{(1),\delta_\Gamma}(p)+\Sigma_{UU}^{(1),\delta_\Gamma}(p).
$$

Recall $I_1=\int_0^1 dx(\frac{d}{2}(p_0\gamma^0-\not{c}\gamma^5)+\frac{1}{2}(2\tilde{c}_{xk}\gamma^k+2c_k\gamma^k\gamma^5))\frac{\Gamma(\frac{2-d}{2})}{(4\pi)^{d/2}\Delta_0^{(2-d)/2}}+\int_0^1 dx\frac{C_0\Gamma(\frac{4-d}{2})}{(4\pi)^{d/2}\Delta_0^{(4-d)/2}}$ in Eq. (C4).

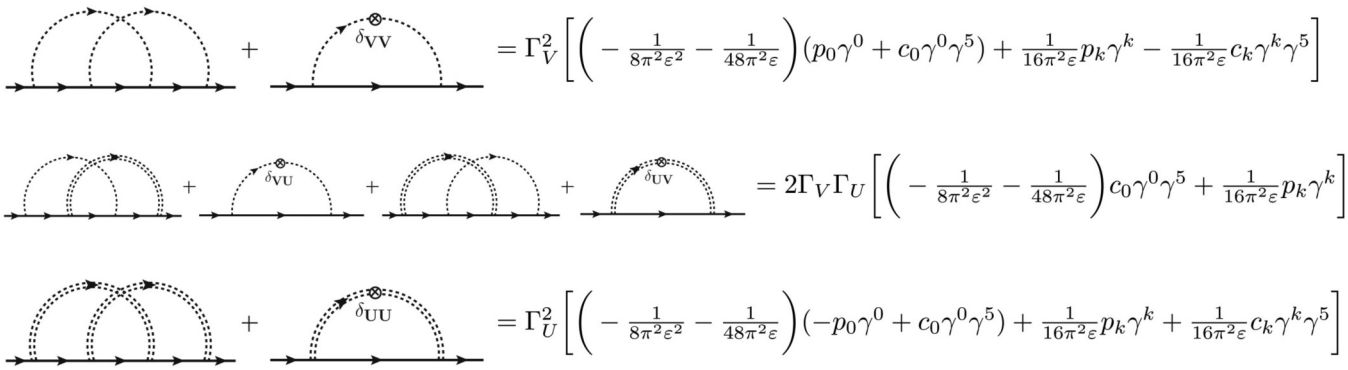

FIG. 12. The result for the crossed diagrams. Each crossed diagram is added consistently by one-loop self-energy diagram made of a tree-level vertex and a vertex-correction counterterm. Note that there are simple poles for c_k, resulting in renormalization of c_k, while the sign difference between Γ_V and Γ_U channels implies that their roles (Γ_V and Γ_U) are different. Also, one may notice that nonlocal divergences of $(\gamma - \ln 4\pi)$ are canceled, which is the result of BPHZ theorem [9], and so the problematic term of $\int_0^1 dx \frac{C_0}{\Delta_0}$ is.

Expanding I_1 about $d = 2+\varepsilon$ and inserting $\delta_{\Gamma V} = \frac{\Gamma_V}{2\pi\varepsilon} + \frac{\Gamma_U}{2\pi\varepsilon}$ and $\delta_{\Gamma U} = -\frac{\Gamma_U}{2\pi\varepsilon} - \frac{\Gamma_V}{2\pi\varepsilon}$ into the above expression, which will be computed in the next section, we obtain

$$\begin{aligned}
\Sigma^{(1),\delta_\Gamma}(p) = {}& \Gamma_V^2\left[-\left(\frac{1}{4\pi^2\varepsilon^2}+\frac{1+\gamma-\ln 4\pi}{8\pi^2\varepsilon}\right)(p_0\gamma^0+c_0\gamma^0\gamma^5)+\frac{1}{8\pi^2\varepsilon}\int_0^1 dx\frac{\bar{C}_0(x)}{\Delta_0(x)}\right]\\
&+\Gamma_V\Gamma_U\left[-\left(\frac{1}{4\pi^2\varepsilon^2}+\frac{1+\gamma-\ln 4\pi}{8\pi^2\varepsilon}\right)(p_0\gamma^0+c_0\gamma^0\gamma^5)+\frac{1}{8\pi^2\varepsilon}\int_0^1 dx\frac{\bar{C}_0(x)}{\Delta_0(x)}\right]\\
&+\Gamma_U\Gamma_V\left[-\left(\frac{1}{4\pi^2\varepsilon^2}+\frac{1+\gamma-\ln 4\pi}{8\pi^2\varepsilon}\right)(-p_0\gamma^0+c_0\gamma^0\gamma^5)-\frac{1}{8\pi^2\varepsilon}\int_0^1 dx\frac{C_0(x)}{\Delta_0(x)}\right]\\
&+\Gamma_U^2\left[-\left(\frac{1}{4\pi^2\varepsilon^2}+\frac{1+\gamma-\ln 4\pi}{8\pi^2\varepsilon}\right)(-p_0\gamma^0+c_0\gamma^0\gamma^5)-\frac{1}{8\pi^2\varepsilon}\int_0^1 dx\frac{C_0(x)}{\Delta_0(x)}\right]+O(1).
\end{aligned}$$

Adding these contributions to the crossed diagrams, we finally obtain

$$\begin{aligned}
\Sigma^{(2),c}(p)+\Sigma^{(1),\delta_\Gamma}(p) = {}& \Gamma_V^2\left[\left(-\frac{1}{8\pi^2\varepsilon^2}-\frac{1}{48\pi^2\varepsilon}\right)(p_0\gamma^0+c_0\gamma^0\gamma^5)+\frac{1}{16\pi^2\varepsilon}p_k\gamma^k-\frac{1}{16\pi^2\varepsilon}c_k\gamma^k\gamma^5\right]\\
&+\Gamma_U^2\left[\left(-\frac{1}{8\pi^2\varepsilon^2}-\frac{1}{48\pi^2\varepsilon}\right)(-p_0\gamma^0+c_0\gamma^0\gamma^5)+\frac{1}{16\pi^2\varepsilon}p_k\gamma^k+\frac{1}{16\pi^2\varepsilon}c_k\gamma^k\gamma^5\right]\\
&+2\Gamma_V\Gamma_U\left[\left(-\frac{1}{8\pi^2\varepsilon^2}-\frac{1}{48\pi^2\varepsilon}\right)c_0\gamma^0\gamma^5+\frac{1}{16\pi^2\varepsilon}p_k\gamma^k\right]+O(1). \qquad \text{(C9)}
\end{aligned}$$

This result is depicted pictorially in Fig. 12.

APPENDIX D: VERTEX CORRECTION

1. Relevant Feynman diagrams

The vertex renormalization can be found from a four-point function of $\mathbf{D}(p,p',q,q') = \langle\psi_p\bar{\psi}_{p'}\psi_q\bar{\psi}_{q'}\rangle$. Performing the perturbative analysis up to the Γ^2 order, we obtain

$$\begin{aligned}
\mathbf{D}(p,p',q,q') = {}& \lim_{R\to 0}\frac{1}{R}\int \mathcal{D}\bar{\psi}\mathcal{D}\psi\left(\psi_p^a\bar{\psi}_{p'}^a\psi_q^a\bar{\psi}_{q'}^a\right)e^{-S_0[\bar{\psi}^\alpha,\psi^\alpha]}e^{\frac{1}{L^3}\sum_{p_j}[\frac{\Gamma_V}{2}(\bar{\psi}_{p_1}^b\gamma^0\psi_{p_2}^b)(\bar{\psi}_{p_3}^c\gamma^0\psi_{p_4}^c)+\frac{\Gamma_U}{2}(\bar{\psi}_{p_1}^b\psi_{p_2}^b)(\bar{\psi}_{p_3}^c\psi_{p_4}^c)]}\delta^{(3)}_{\boldsymbol{p}_1-\boldsymbol{p}_2,\boldsymbol{p}_3-\boldsymbol{p}_4}\delta_{p_1^0p_2^0}\delta_{p_3^0p_4^0}\\
\simeq {}& \lim_{R\to 0}\frac{1}{R}\int \mathcal{D}\bar{\psi}\mathcal{D}\psi e^{-S_0[\bar{\psi}^\alpha,\psi^\alpha]}\left[\psi_p^a\bar{\psi}_{p'}^a\psi_q^a\bar{\psi}_{q'}^a+\frac{\Gamma_V}{2L^3}\sum_{p_j}\left(\psi_p^a\bar{\psi}_{p'}^a\psi_q^a\bar{\psi}_{q'}^a\right)\left(\bar{\psi}_{p_1}^b\gamma^0\psi_{p_2}^b\bar{\psi}_{p_3}^c\gamma^0\psi_{p_4}^c\right)\delta^{(3)}_{\boldsymbol{p}_1-\boldsymbol{p}_2,\boldsymbol{p}_3-\boldsymbol{p}_4}\right.\\
&\times\delta_{p_1^0p_2^0}\delta_{p_3^0p_4^0}+\frac{\Gamma_U}{2L^3}\sum_{p_j}\left(\psi_p^a\bar{\psi}_{p'}^a\psi_q^a\bar{\psi}_{q'}^a\right)\left(\bar{\psi}_{p_1}^b\psi_{p_2}^b\bar{\psi}_{p_3}^c\psi_{p_4}^c\right)\delta^{(3)}_{\boldsymbol{p}_1-\boldsymbol{p}_2,\boldsymbol{p}_3-\boldsymbol{p}_4}\delta_{p_1^0p_2^0}\delta_{p_3^0p_4^0}+\frac{\Gamma_V^2}{8(L^3)^2}\sum_{p_jp_j'}\left(\psi_p^a\bar{\psi}_{p'}^a\psi_q^a\bar{\psi}_{q'}^a\right)\\
&\left.\times\left(\bar{\psi}_{p_1}^b\gamma^0\psi_{p_2}^b\bar{\psi}_{p_3}^c\gamma^0\psi_{p_4}^c\right)\left(\bar{\psi}_{p_1'}^{b'}\gamma^0\psi_{p_2'}^{b'}\bar{\psi}_{p_3'}^{c'}\gamma^0\psi_{p_4'}^{c'}\right)\delta^{(3)}_{\boldsymbol{p}_1-\boldsymbol{p}_2,\boldsymbol{p}_3-\boldsymbol{p}_4}\delta_{p_1^0p_2^0}\delta_{p_3^0p_4^0}\delta^{(3)}_{\boldsymbol{p}_1'-\boldsymbol{p}_2',\boldsymbol{p}_3'-\boldsymbol{p}_4'}\delta_{p_1'^0p_2'^0}\delta_{p_3'^0p_4'^0}\right]
\end{aligned}$$

$$+\frac{\Gamma_U^2}{8(L^3)^2}\sum_{p_j p_j'}\left(\psi^a_p\bar\psi^a_{p'}\psi^a_q\bar\psi^a_{q'}\right)\left(\bar\psi^b_{p_1}\psi^b_{p_2}\bar\psi^c_{p_3}\psi^c_{p_4}\right)\left(\bar\psi^{b'}_{p_1'}\psi^{b'}_{p_2'}\bar\psi^{c'}_{p_3'}\psi^{c'}_{p_4'}\right)\delta^{(3)}_{\boldsymbol{p}_1-\boldsymbol{p}_2,\boldsymbol{p}_3-\boldsymbol{p}_4}\delta_{p_1^0p_2^0}\delta_{p_3^0p_4^0}\delta^{(3)}_{\boldsymbol{p}_1'-\boldsymbol{p}_2',\boldsymbol{p}_3'-\boldsymbol{p}_4'}\delta_{p_1'^0p_2'^0}\delta_{p_3'^0p_4'^0}$$

$$+\frac{\Gamma_V\Gamma_U}{4(L^3)^2}\sum_{p_j p_j'}\left(\psi^a_p\bar\psi^a_{p'}\psi^a_q\bar\psi^a_{q'}\right)\left(\bar\psi^b_{p_1}\gamma^0\psi^b_{p_2}\bar\psi^c_{p_3}\gamma^0\psi^c_{p_4}\right)\left(\bar\psi^{b'}_{p_1'}\psi^{b'}_{p_2'}\bar\psi^{c'}_{p_3'}\psi^{c'}_{p_4'}\right)$$

$$\times\,\delta^{(3)}_{\boldsymbol{p}_1-\boldsymbol{p}_2,\boldsymbol{p}_3-\boldsymbol{p}_4}\delta_{p_1^0p_2^0}\delta_{p_3^0p_4^0}\delta^{(3)}_{\boldsymbol{p}_1'-\boldsymbol{p}_2',\boldsymbol{p}_3'-\boldsymbol{p}_4'}\delta_{p_1'^0p_2'^0}\delta_{p_3'^0p_4'^0}\Bigg].$$

Among the first-order contributions, fully connected diagrams give scattering elements (Fig. 13). The four-point function and the scattering matrix element at the tree level are

$$M^{(0)}(p,p;q)\equiv M_V^{(0)}(p,p;q)+M_U^{(0)}(p,p;q)=2\Gamma_V(\gamma^0\otimes\gamma^0)+2\Gamma_V(I_{4\times4}\otimes I_{4\times4}). \tag{D1}$$

Among the second-order contributions, only diagrams fully connected with the external lines survive in the replica limit of $R\to0$ and give scattering matrix elements. Thus, the scattering matrix elements in the second order are given by (Fig. 14)

$$\begin{aligned}
\mathcal{M}^{(1)}_{ph}&=\frac{2\Gamma_V^2}{L^3}\sum_l\gamma^0G(p-l)\gamma^0\otimes\gamma^0G(p'-l-q)\gamma^0\delta_{l^0}+\frac{2\Gamma_V\Gamma_U}{L^3}\sum_l\gamma^0G(p-l)\otimes G(p'-l-q)\gamma^0\delta_{l^0}\\
&\quad+\frac{2\Gamma_U\Gamma_V}{L^3}\sum_l G(p-l)\gamma^0\otimes\gamma^0G(p'-l-q)\delta_{l^0}+\frac{2\Gamma_U^2}{L^3}\sum_l G(p-l)\otimes G(p'-l-q)\delta_{l^0},\\
&\equiv\mathcal{M}^{ph}_{VV}+\mathcal{M}^{ph}_{VU}+\mathcal{M}^{ph}_{UV}+\mathcal{M}^{ph}_{UU}\\
\mathcal{M}^{(1)}_{pp}&=\frac{2\Gamma_V^2}{L^3}\sum_l\gamma^0G(p-l)\gamma^0\otimes\gamma^0G(p'+l)\gamma^0\delta_{l^0}+\frac{2\Gamma_V\Gamma_U}{L^3}\sum_l\gamma^0G(p-l)\otimes\gamma^0G(p'+l)\delta_{l^0}\\
&\quad+\frac{2\Gamma_U\Gamma_V}{L^3}\sum_l G(p-l)\gamma^0\otimes G(p'+l)\gamma^0\delta_{l^0}+\frac{2\Gamma_U^2}{L^3}\sum_l G(p-l)\otimes G(p'+l)\delta_{l^0},\\
&\equiv\mathcal{M}^{pp}_{VV}+\mathcal{M}^{pp}_{VU}+\mathcal{M}^{pp}_{UV}+\mathcal{M}^{pp}_{UU}\\
\mathcal{M}^{(1)}_{\rm ver}&=\frac{2\Gamma_V^2}{L^3}\sum_l\gamma^0G(p-l)\gamma^0G(p+q-l)\gamma^0\otimes\gamma^0\delta_{l^0}+\frac{2\Gamma_V\Gamma_U}{L^3}\sum_l\gamma^0G(p-l)G(p+q-l)\gamma^0\otimes I_{4\times4}\delta_{l^0}\\
&\quad+\frac{2\Gamma_U\Gamma_V}{L^3}\sum_l G(p-l)\gamma^0G(p+q-l)\otimes\gamma^0\delta_{l^0}+\frac{2\Gamma_U^2}{L^3}\sum_l G(p-l)G(p+q-l)\otimes I_{4\times4}\delta_{l^0},\\
&\equiv\mathcal{M}^{\rm ver}_{VV}+\mathcal{M}^{\rm ver}_{VU}+\mathcal{M}^{\rm ver}_{UV}+\mathcal{M}^{\rm ver}_{UU},
\end{aligned}$$

where *ph*, *pp*, and *ver* represent particle-hole, particle-particle, and vertex, respectively.

2. Evaluation of relevant diagrams

a. Particle-hole channel

First, we evaluate the particle-hole diagrams (the first line in Fig. 14)

$$\begin{aligned}
\mathcal{M}^{(1)}_{ph}&=2\Gamma_V^2I_{2ph}[M_1=M_2=\gamma^0]+2\Gamma_V\Gamma_UI_{2ph}[M_1=\gamma^0,M_2=I_{4\times4}]\\
&\quad+2\Gamma_U\Gamma_VI_{2ph}[M_1=I_{4\times4},M_2=\gamma^0]+2\Gamma_U^2I_{2ph}[M_1=M_2=I_{4\times4}],
\end{aligned}$$

where I_{2ph} is given by ($\boldsymbol{k}\equiv\boldsymbol{p}-\boldsymbol{p}'+\boldsymbol{q}$)

$$\begin{aligned}
I_{2ph}&=\int\frac{d^{d+1}l}{(2\pi)^{d+1}}2\pi\delta(l_0)M_1G(p-l)M_2\otimes M_2G(p'-l-q)M_1\\
&=\int\frac{d^d\boldsymbol{l}}{(2\pi)^d}M_1G(p_0,\boldsymbol{p}-\boldsymbol{l})M_2\otimes M_2G(p_0'-q_0,\boldsymbol{p}'-\boldsymbol{l}-\boldsymbol{q})M_1\\
&=\int\frac{d^d\boldsymbol{l}}{(2\pi)^d}M_1G(p_0,-\boldsymbol{l})M_2\otimes M_2G(p_0'-q_0,-\boldsymbol{l}-\boldsymbol{k})M_1.
\end{aligned}$$

Using Eq. (B1), we have

$$I_{2ph} = \int_0^1 dx \int_0^1 dy \int \frac{d^d \boldsymbol{l}}{(2\pi)^d} M_1 \frac{-\boldsymbol{l}^2 l_i \gamma^i + \boldsymbol{l}^2(p_0\gamma^0 - \not{c}\gamma^5) + l_i l_j(-2c^i\gamma^j\gamma^5) - l_i f_1^i(p_0) + f_0(p_0)}{[(\boldsymbol{l} - (1-2x)\boldsymbol{c})^2 + \Delta_0(p_0;x)]^2} M_2 \otimes M_2$$
$$\times \frac{-(\boldsymbol{l}+\boldsymbol{k})^2(l_j+k_j)\gamma^j + (\boldsymbol{l}+\boldsymbol{k})^2((p_0'-q_0)\gamma^0 - \not{c}\gamma^5) + (l_i+k_i)(l_j+k_j)(-2c^i\gamma^j\gamma^5) - (l_i+k_i)f_1^i(p_0'-q_0) + f_0(p_0'-q_0)}{[(\boldsymbol{l}+\boldsymbol{k}-(1-2y)\boldsymbol{c})^2 + \Delta_0(p_0'-q_0;y)]^2} M_1.$$

Despite this complicated expression, only the product of the l-cubic terms contributes to renormalization by the same reason that we considered in Eq. (C8). Keeping this term only, we obtain

$$I_{2ph} \simeq \int_0^1 dx \int_0^1 dy \int \frac{d^d \boldsymbol{l}}{(2\pi)^d} \frac{\boldsymbol{l}^2(\boldsymbol{l}+\boldsymbol{k})^2 l_i(l_j+k_j)(M_1\gamma^i M_2 \otimes M_2\gamma^j M_1)}{[(\boldsymbol{l}-(1-2x)\boldsymbol{c})^2 + \Delta_0(x)]^2[(\boldsymbol{l}+\boldsymbol{k}-(1-2y)\boldsymbol{c})^2 + \Delta_0(y)]^2}$$
$$= \int_0^1 dx \int_0^1 dy \int_0^1 dz 6z(1-z) \int \frac{d^d \boldsymbol{l}}{(2\pi)^d} \frac{\boldsymbol{l}^2(\boldsymbol{l}+\boldsymbol{k})^2 l_i(l_j+k_j)(M_1\gamma^i M_2 \otimes M_2\gamma^j M_1)}{[\boldsymbol{l}'^2 + \Delta_1(\boldsymbol{k};x,y,z)]^4},$$

where $\Delta_1 = z(1-z)(\boldsymbol{k} + 2(y-x)\boldsymbol{c})^2 + (1-z)\Delta_0(x) + z\Delta_0(y)$ and $\boldsymbol{l}' = \boldsymbol{l} + z\boldsymbol{k} - z(1-2y)\boldsymbol{c} - (1-z)(1-2x)\boldsymbol{c}$.

Renaming momentum as $\boldsymbol{l}' \to \boldsymbol{l}$ and keeping only a relevant term again, we reach the following expression

$$I_{2ph} = (M_1\gamma^i M_2 \otimes M_2\gamma^j M_1) \int_0^1 dx \int_0^1 dy \int_0^1 dz 6z(1-z) \int \frac{d^d \boldsymbol{l}}{(2\pi)^d} \frac{(\boldsymbol{l}^2)^2 l_i l_j}{[\boldsymbol{l}^2 + \Delta_1]^4}$$
$$= (M_1\gamma^i M_2 \otimes M_2\gamma^i M_1) \int_0^1 dx \int_0^1 dy \int_0^1 dz z(1-z) \frac{(d+4)(d+2)}{32\pi} \Gamma\left(\frac{2-d}{2}\right)\left(\frac{\Delta_1}{4\pi}\right)^{\frac{d-2}{2}}$$
$$= -\frac{1}{4\pi\varepsilon}(M_1\gamma^i M_2 \otimes M_2\gamma^i M_1) + O(1).$$

Thus, the scattering matrix element for the particle-hole diagrams is

$$\mathcal{M}_{ph}^{(1)} = -\frac{\Gamma_V^2}{2\pi\varepsilon}(\gamma^i \otimes \gamma^i) + \frac{\Gamma_V\Gamma_U}{\pi\varepsilon}(\gamma^0\gamma^i \otimes \gamma^0\gamma^i) - \frac{\Gamma_U^2}{2\pi\varepsilon}(\gamma^i \otimes \gamma^i) + O(1). \tag{D2}$$

b. Particle-particle channel

Next, we evaluate the particle-particle diagrams (the second line in Fig. 14)

$$\mathcal{M}_{pp}^{(1)} = 2\Gamma_V^2 I_{2pp}[M_1 = M_2 = \gamma^0] + 2\Gamma_V\Gamma_U I_{2pp}[M_1 = \gamma^0, M_2 = I_{4\times4}]$$
$$+ 2\Gamma_U\Gamma_V I_{2pp}[M_1 = I_{4\times4}, M_2 = \gamma^0] + 2\Gamma_U^2 I_{2pp}[M_1 = M_2 = I_{4\times4}],$$

where I_{2pp} is given by ($\boldsymbol{k} \equiv \boldsymbol{p} + \boldsymbol{p}'$)

$$I_{2pp} = \int \frac{d^{d+1}l}{(2\pi)^{d+1}} 2\pi\delta(l_0) M_1 G(p-l) M_2 \otimes M_1 G(p'+l) M_2$$
$$= \int \frac{d^d \boldsymbol{l}}{(2\pi)^d} M_1 G(p_0, \boldsymbol{p} - \boldsymbol{l}) M_2 \otimes M_1 G(p_0', \boldsymbol{p}' + \boldsymbol{l}) M_2$$
$$= \int \frac{d^d \boldsymbol{l}}{(2\pi)^d} M_1 G(p_0, -\boldsymbol{l}) M_2 \otimes M_1 G(p_0', \boldsymbol{l} + \boldsymbol{k}) M_2.$$

The analysis is quite similar with that of the particle-hole channel. Keeping only a relevant term, we have

$$I_{2pp} \simeq \int_0^1 dx \int_0^1 dy \int \frac{d^d \boldsymbol{l}}{(2\pi)^d} \frac{-\boldsymbol{l}^2(\boldsymbol{l}+\boldsymbol{k})^2 l_i(l_j+k_j)(M_1\gamma^i M_2 \otimes M_1\gamma^j M_2)}{[(\boldsymbol{l}-(1-2x)\boldsymbol{c})^2 + \Delta_0(x)]^2[(\boldsymbol{l}+\boldsymbol{k}+(1-2y)\boldsymbol{c})^2 + \Delta_0(y)]^2}$$
$$= -\int_0^1 dx \int_0^1 dy \int_0^1 dz 6z(1-z) \int \frac{d^d \boldsymbol{l}}{(2\pi)^d} \frac{\boldsymbol{l}^2(\boldsymbol{l}+\boldsymbol{k})^2 l_i(l_j+k_j)(M_1\gamma^i M_2 \otimes M_1\gamma^j M_2)}{[\boldsymbol{l}'^2 + \Delta_1(\boldsymbol{k};x,y,z)]^4},$$

where $\Delta_1 = z(1-z)(\boldsymbol{k} + 2(1-x-y)\boldsymbol{c})^2 + (1-z)\Delta_0(x) + z\Delta_0(y)$ and $\boldsymbol{l}' = \boldsymbol{l} + z\boldsymbol{k} + z(1-2y)\boldsymbol{c} - (1-z)(1-2x)\boldsymbol{c}$. Note a minus sign in front of the integral that essentially originates from the opposite sign in the loop-momentum of the two propagators. Due to this sign difference, the contribution from the particle-particle diagram will cancel that of the particle-hole diagram.

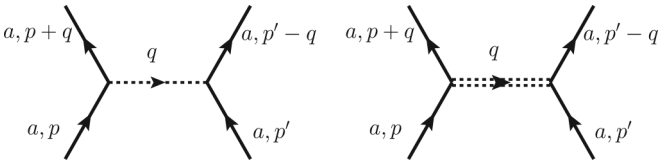

FIG. 13. Tree-level vertex. There are two contributions from intravalley and intervalley scattering.

The remaining calculation is the same as before. As a result, we reach the following expression:

$$I_{2pp} = +\frac{1}{4\pi\varepsilon}(M_1\gamma^i M_2 \otimes M_1\gamma^i M_2) + O(1).$$

Thus, the scattering matrix elements for the particle-particle diagrams is

$$\mathcal{M}^{(1)}_{pp} = \frac{\Gamma_V^2}{2\pi\varepsilon}(\gamma^i \otimes \gamma^i) + \frac{\Gamma_V\Gamma_U}{\pi\varepsilon}(\gamma^0\gamma^i \otimes \gamma^0\gamma^i) + \frac{\Gamma_U^2}{2\pi\varepsilon}(\gamma^i \otimes \gamma^i) + O(1). \tag{D3}$$

c. Vertex channel

Lastly, we evaluate the vertex diagrams (the third line in Fig. 14)

$$\begin{aligned}\mathcal{M}^{(1)}_{\text{ver}} = {} & 2\Gamma_V^2 I_{2\text{ver}}[M_1 = M_2 = \gamma^0] + 2\Gamma_V\Gamma_U I_{2\text{ver}}[M_1 = \gamma^0, M_2 = I_{4\times4}] \\ & + 2\Gamma_U\Gamma_V I_{2\text{ver}}[M_1 = I_{4\times4}, M_2 = \gamma^0] + 2\Gamma_U^2 I_{2\text{ver}}[M_1 = M_2 = I_{4\times4}],\end{aligned}$$

where $I_{2\text{ver}}$ is given by

$$\begin{aligned}I_{2\text{ver}} &= \int \frac{d^{d+1}l}{(2\pi)^{d+1}} M_1 G(p-l) M_2 G(p+q-l) M_1 \otimes M_2 \delta_{l^0 0} \\ &= \int \frac{d^d \boldsymbol{l}}{(2\pi)^d} M_1 G(p_0, \boldsymbol{p}-\boldsymbol{l}) M_2 G(p_0+q_0, \boldsymbol{p}+\boldsymbol{q}-\boldsymbol{l}) M_1 \otimes M_2 \\ &= \int \frac{d^d \boldsymbol{l}}{(2\pi)^d} M_1 G(p_0, -\boldsymbol{l}) M_2 G(p_0+q_0, -\boldsymbol{l}+\boldsymbol{q}) M_1 \otimes M_2.\end{aligned}$$

The analysis is also similar with the particle-hole case except for the fact that $\otimes$ are not located between propagators.

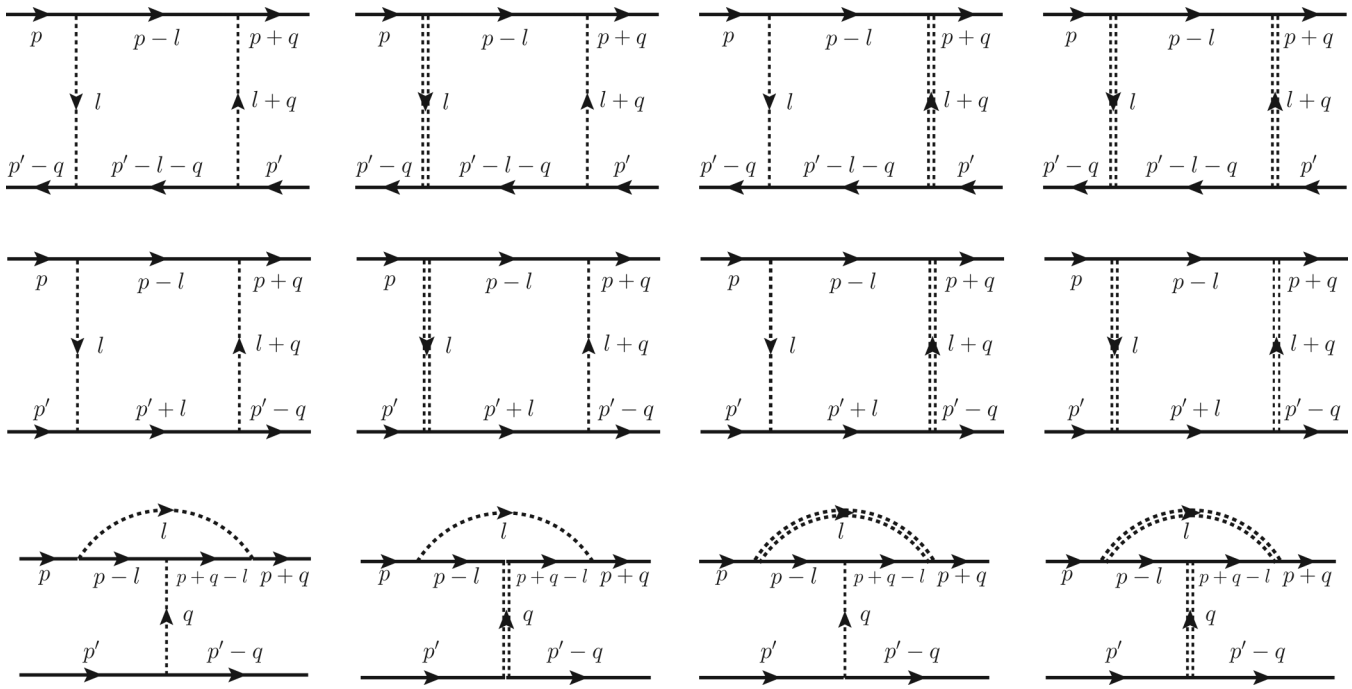

FIG. 14. Vertex corrections in the second order. There are three distinct types of diagrams, i.e., particle-hole, particle-particle, and vertex diagrams. Diagrams in each type are distinguished by interaction vertices (two intravalley scattering, one intravalley, and one intervalley scattering, etc.). So, totally there are twelve diagrams for the second-order vertex corrections.

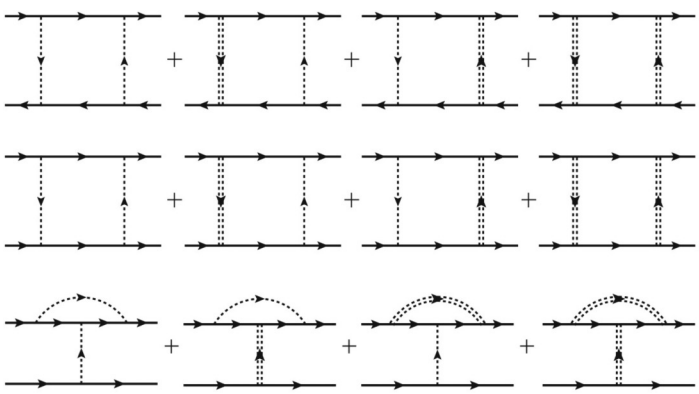

FIG. 15. The result for the vertex corrections in the second order. Note that the contribution from the particle-hole diagrams (the first line) will be canceled to that of the particle-particle diagrams (the second line). A novel coupling term of $\gamma^0\gamma^i$ appears, but does not concern us here. As a result, vertex diagrams (the third line) participate in renormalization of intravalley scattering (Γ_V) and intervalley scattering (Γ_U). Note the sign difference in the two factors, which results in the distinction between two types of scatterings. That is, intervalley scattering becomes relevant while intravalley scattering irrelevant in the low-energy physics.

Keeping only a relevant term, we have

$$\begin{aligned} I_{2\text{ver}} &\simeq \int_0^1 dx \int_0^1 dy \int \frac{d^d\boldsymbol{l}}{(2\pi)^d} \frac{\boldsymbol{l}^2(\boldsymbol{l}-\boldsymbol{q})^2 l_i(l_j-q_j)(M_1\gamma^i M_2\gamma^j M_1 \otimes M_2)}{[(\boldsymbol{l}-(1-2x)\boldsymbol{c})^2+\Delta_0(x)]^2[(\boldsymbol{l}-\boldsymbol{q}-(1-2y)\boldsymbol{c})^2+\Delta_0(y)]^2} \\ &= \int_0^1 dx \int_0^1 dy \int_0^1 dz 6z(1-z) \int \frac{d^d\boldsymbol{l}}{(2\pi)^d} \frac{\boldsymbol{l}^2(\boldsymbol{l}-\boldsymbol{q})^2 l_i(l_j-q_j)(M_1\gamma^i M_2\gamma^j M_1 \otimes M_2)}{[\boldsymbol{l}'^2+\Delta_1(\boldsymbol{q};x,y,z)]^4}, \end{aligned}$$

where $\Delta_1 = z(1-z)(\boldsymbol{q}+2(x-y)\boldsymbol{c})^2 + (1-z)\Delta_0(x) + z\Delta_0(y)$ and $\boldsymbol{l}' = \boldsymbol{l} - z\boldsymbol{q} - z(1-2y)\boldsymbol{c} - (1-z)(1-2x)\boldsymbol{c}$.

Renaming momentum as $\boldsymbol{l}' \to \boldsymbol{l}$ and keeping only a relevant term again, we reach the following expression

$$\begin{aligned} I_{2\text{ver}} &= (M_1\gamma^i M_2\gamma^j M_1 \otimes M_2) \int_0^1 dx \int_0^1 dy \int_0^1 dz 6z(1-z) \int \frac{d^d\boldsymbol{l}}{(2\pi)^d} \frac{(\boldsymbol{l}^2)^2 l_i l_j}{[\boldsymbol{l}^2+\Delta_1]^4} \\ &= (M_1\gamma^i M_2\gamma^i M_1 \otimes M_2) \int_0^1 dx \int_0^1 dy \int_0^1 dz z(1-z) \frac{(d+4)(d+2)}{32\pi} \Gamma\left(\frac{2-d}{2}\right)\left(\frac{\Delta_1}{4\pi}\right)^{\frac{d-2}{2}} \\ &= -\frac{M_1\gamma^i M_2\gamma^i M_1 \otimes M_2}{4\pi\varepsilon} + O(1). \end{aligned}$$

Thus, the scattering matrix element for the vertex diagrams is

$$\mathcal{M}_{\text{ver}}^{(1)} = -\frac{\Gamma_V^2}{\pi\varepsilon}(\gamma^0 \otimes \gamma^0) + \frac{\Gamma_V\Gamma_U}{\pi\varepsilon}(I_{4\times4} \otimes I_{4\times4}) - \frac{\Gamma_U\Gamma_V}{\pi\varepsilon}(\gamma^0 \otimes \gamma^0) + \frac{\Gamma_U^2}{\pi\varepsilon}(I_{4\times4} \otimes I_{4\times4}) + O(1), \tag{D4}$$

where the result is depicted pictorially in Fig. 15.

APPENDIX E: RENORMALIZATION GROUP EQUATIONS

Combining Eqs. (C5), (C7), and (C9) in the following way

$$\begin{aligned} &\Sigma^{(1)}(p) + (\Sigma^{(2),r}(p) + \Sigma^{(1),\delta_\psi}(p)) + (\Sigma^{(2),c}(p) + \Sigma^{(1),\delta_\Gamma}(p)) + (\text{propagator counterterms}) \\ &= -\frac{\Gamma_V}{2\pi\varepsilon}(p_0\gamma^0 + c_0\gamma^0\gamma^5) - \frac{\Gamma_U}{2\pi\varepsilon}(p_0\gamma^0 - c_0\gamma^0\gamma^5) \\ &\quad + \frac{\Gamma_V^2}{8\pi^2\varepsilon}(p_0\gamma^0 + c_0\gamma^0\gamma^5) + \frac{\Gamma_U^2}{8\pi^2\varepsilon}(p_0\gamma^0 + c_0\gamma^0\gamma^5) + \frac{2\Gamma_V\Gamma_U}{8\pi^2\varepsilon}(p_0\gamma^0 - c_0\gamma^0\gamma^5) \\ &\quad + \Gamma_V^2\left[\left(-\frac{1}{8\pi^2\varepsilon^2} - \frac{1}{48\pi^2\varepsilon}\right)(p_0\gamma^0 + c_0\gamma^0\gamma^5) + \frac{1}{16\pi^2\varepsilon}p_k\gamma^k - \frac{1}{16\pi^2\varepsilon}c_k\gamma^k\gamma^5\right] \\ &\quad + \Gamma_U^2\left[\left(-\frac{1}{8\pi^2\varepsilon^2} - \frac{1}{48\pi^2\varepsilon}\right)(-p_0\gamma^0 + c_0\gamma^0\gamma^5) + \frac{1}{16\pi^2\varepsilon}p_k\gamma^k + \frac{1}{16\pi^2\varepsilon}c_k\gamma^k\gamma^5\right] \\ &\quad + 2\Gamma_V\Gamma_U\left[\left(-\frac{1}{8\pi^2\varepsilon^2} - \frac{1}{48\pi^2\varepsilon}\right)c_0\gamma^0\gamma^5 + \frac{1}{16\pi^2\varepsilon}p_k\gamma^k\right] + O(1) + \left(\delta_\psi^\omega p_0\gamma^0 + \delta_\psi^{\boldsymbol{k}} p_k\gamma^k + \delta_{c0}c_0\gamma^0\gamma^5 + \delta_{\boldsymbol{c}}c_k\gamma^k\gamma^5\right), \end{aligned}$$

we find propagator counter terms in Eq. (14)

$$\delta_\psi^\omega = \frac{\Gamma_V+\Gamma_U}{2\pi\varepsilon} - \frac{(\Gamma_V+\Gamma_U)^2}{8\pi^2\varepsilon} + \frac{\Gamma_V^2-\Gamma_U^2}{48\pi^2\varepsilon}, \quad \delta_\psi^{\boldsymbol{k}} = -\frac{(\Gamma_V+\Gamma_U)^2}{16\pi^2\varepsilon},$$
$$\delta_{c0} = \frac{\Gamma_V-\Gamma_U}{2\pi\varepsilon} - \frac{(\Gamma_V-\Gamma_U)^2}{8\pi^2\varepsilon} + \frac{(\Gamma_V+\Gamma_U)^2}{48\pi^2\varepsilon}, \quad \delta_{\boldsymbol{c}} = \frac{\Gamma_V^2-\Gamma_U^2}{16\pi^2\varepsilon}.$$

Similarly, combining Eqs. (D2)–(D4) as follows:

$$\begin{aligned}
&\mathcal{M}_{ph}^{(1)} + \mathcal{M}_{pp}^{(1)} + \mathcal{M}_{\rm ver}^{(1)} + 4\times\delta_{\Gamma V}\frac{\Gamma_V}{2}(\gamma^0\otimes\gamma^0) + 4\times\delta_{\Gamma U}\frac{\Gamma_U}{2}(I_{4\times4}\otimes I_{4\times4}) + 4\times\frac{\delta_{\Gamma T}}{2}(\gamma^0\gamma^i\otimes\gamma^0\gamma^i)\\
&= -\frac{\Gamma_V^2}{2\pi\varepsilon}(\gamma^i\otimes\gamma^i) + \frac{\Gamma_V\Gamma_U}{\pi\varepsilon}(\gamma^0\gamma^i\otimes\gamma^0\gamma^i) - \frac{\Gamma_U^2}{2\pi\varepsilon}(\gamma^i\otimes\gamma^i) + \frac{\Gamma_V^2}{2\pi\varepsilon}(\gamma^i\otimes\gamma^i) + \frac{\Gamma_V\Gamma_U}{\pi\varepsilon}(\gamma^0\gamma^i\otimes\gamma^0\gamma^i) + \frac{\Gamma_U^2}{2\pi\varepsilon}(\gamma^i\otimes\gamma^i)\\
&\quad -\frac{\Gamma_V^2}{\pi\varepsilon}(\gamma^0\otimes\gamma^0) + \frac{\Gamma_V\Gamma_U}{\pi\varepsilon}(I_{4\times4}\otimes I_{4\times4}) - \frac{\Gamma_U\Gamma_V}{\pi\varepsilon}(\gamma^0\otimes\gamma^0) + \frac{\Gamma_U^2}{\pi\varepsilon}(I_{4\times4}\otimes I_{4\times4}) + O(1)\\
&\quad +2\delta_{\Gamma V}\Gamma_V(\gamma^0\otimes\gamma^0) + 2\delta_{\Gamma U}\Gamma_U(I_{4\times4}\otimes I_{4\times4}) + 2\delta_{\Gamma T}(\gamma^0\gamma^i\otimes\gamma^0\gamma^i),
\end{aligned}$$

we find vertex counter terms in Eq. (14)

$$\delta_{\Gamma V} = \frac{\Gamma_V}{2\pi\varepsilon} + \frac{\Gamma_U}{2\pi\varepsilon}, \quad \delta_{\Gamma U} = -\frac{\Gamma_U}{2\pi\varepsilon} - \frac{\Gamma_V}{2\pi\varepsilon}, \quad \delta_{\Gamma T} = -\frac{\Gamma_V\Gamma_U}{\pi\varepsilon}.$$

As a result, we obtain the renormalization factors:

$$\begin{aligned}
Z_\psi^\omega &\simeq \exp\left[-\frac{\Gamma_V+\Gamma_U}{2\pi}\ln M + \frac{5\Gamma_V^2+12\Gamma_V\Gamma_U+7\Gamma_U^2}{48\pi^2}\ln M\right],\\
Z_\psi^{\boldsymbol{k}} &\simeq \exp\left[\frac{(\Gamma_V+\Gamma_U)^2}{16\pi^2}\ln M\right],\\
Z_{c0} &\simeq \exp\left[-\frac{\Gamma_V-\Gamma_U}{2\pi}\ln M + \frac{5\Gamma_V^2-14\Gamma_V\Gamma_U+5\Gamma_U^2}{48\pi^2}\ln M\right],\\
Z_{\boldsymbol{c}} &\simeq \exp\left[-\frac{\Gamma_V^2-\Gamma_U^2}{16\pi^2}\ln M\right],\\
Z_{\Gamma V} &\simeq \exp\left[-\frac{\Gamma_V+\Gamma_U}{2\pi}\ln M\right],\\
Z_{\Gamma U} &\simeq \exp\left[\frac{\Gamma_V+\Gamma_U}{2\pi}\ln M\right],
\end{aligned} \tag{E1}$$

where we have replaced $\frac{1}{\varepsilon}$ with a cutoff scale, $\ln\frac{1}{M}$, and approximated the renormalization factor as $Z = 1+\delta \simeq \exp(\delta)$.

Recall the relations between the bare and renormalized quantities: $\Gamma_V = M^{d-2}(Z_\psi^\omega)^2(Z_{\Gamma V})^{-1}\Gamma_{BV}, \Gamma_U = M^{d-2}(Z_\psi^\omega)^2(Z_{\Gamma U})^{-1}\Gamma_U, v_R = Z_\psi^\omega(Z_\psi^{\boldsymbol{k}})^{-1}v_B c_{R0} = M^{-1}Z_\psi^\omega(Z_{c0})^{-1}c_{B0}$, and $c_{Rk} = M^{-1}Z_\psi^\omega(Z_{\boldsymbol{c}})^{-1}c_{Bk}$. Based on these equations, it is straightforward to find the renormalization group equations

$$\begin{aligned}
\frac{d\ln\Gamma_V}{d\ln M} &= d-2+2\frac{d\ln Z_\psi^\omega}{d\ln M} - \frac{d\ln Z_{\Gamma V}}{d\ln M},\\
\frac{d\ln\Gamma_U}{d\ln M} &= d-2+2\frac{d\ln Z_\psi^\omega}{d\ln M} - \frac{d\ln Z_{\Gamma U}}{d\ln M},\\
\frac{d\ln v}{d\ln M} &= \frac{d\ln Z_\psi^\omega}{d\ln M} - \frac{d\ln Z_\psi^{\boldsymbol{k}}}{d\ln M},\\
\frac{d\ln c_0}{d\ln M} &= -1+\frac{d\ln Z_\psi^\omega}{d\ln M} - \frac{d\ln Z_{c0}}{d\ln M},\\
\frac{d\ln c_k}{d\ln M} &= -1+\frac{d\ln Z_\psi^\omega}{d\ln M} - \frac{d\ln Z_{\boldsymbol{c}}}{d\ln M}.
\end{aligned} \tag{E2}$$

Substituting the results of (E1) into Eq. (E2), we obtain the renormalization group equations [Eq. (15)]

$$\begin{aligned}
\frac{d\Gamma_V}{d\ln M} &= \Gamma_V\left[1-\frac{\Gamma_V+\Gamma_U}{2\pi}+\frac{(\Gamma_V+\Gamma_U)(5\Gamma_V+7\Gamma_U)}{24\pi^2}\right],\\
\frac{d\Gamma_U}{d\ln M} &= \Gamma_U\left[1-\frac{3(\Gamma_V+\Gamma_U)}{2\pi}+\frac{(\Gamma_V+\Gamma_U)(5\Gamma_V+7\Gamma_U)}{24\pi^2}\right],\\
\frac{dv}{d\ln M} &= v\left[-\frac{\Gamma_V+\Gamma_U}{2\pi}+\frac{(\Gamma_V+\Gamma_U)(\Gamma_V+2\Gamma_U)}{24\pi^2}\right],\\
\frac{dc_0}{d\ln M} &= c_0\left[-1-\frac{\Gamma_U}{\pi}+\frac{\Gamma_U(\Gamma_U+13\Gamma_V)}{24\pi^2}\right],\\
\frac{dc_k}{d\ln M} &= c_k\left[-1-\frac{\Gamma_V+\Gamma_U}{2\pi}+\frac{(\Gamma_V+\Gamma_U)(2\Gamma_V+\Gamma_U)}{12\pi^2}\right].
\end{aligned}$$

We notice that Γ_V and Γ_U affect renormalization of the other parameters, but the reverse way is not the case. In other

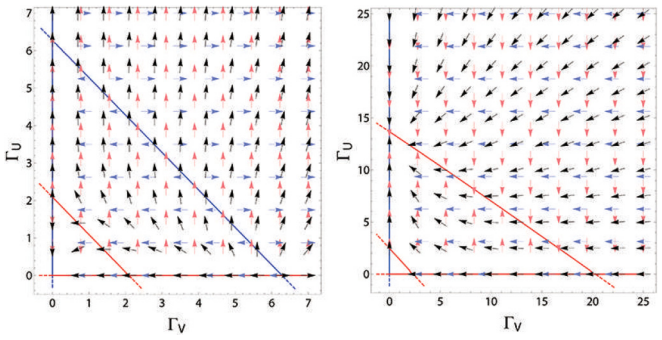

FIG. 16. Topography of the renormalization group equations for Γ_V and Γ_U. At each point red, blue, and black arrows denote the direction in which Γ_V, Γ_U and (Γ_V,Γ_U) are heading as lowering the scale of the system. In the left figure, where only one-loop corrections are included, there are two critical lines each for Γ_U (the red line) and Γ_V (the blue line). In the right figure, where two-loop corrections are also included, there appears another critical line for Γ_U while the critical line for Γ_V disappears. As a result, the direction of Γ_V remains negative so there are two nonzero fixed points on the line of $\Gamma_V = 0$.

words, Γ_V and Γ_U determine renormalization effects of all parameters, including themselves. In this respect we focus first on the equations for Γ_V and Γ_U:

$$\frac{d\Gamma_V}{d\ln M} = \Gamma_V\left[1 - \frac{\Gamma_V+\Gamma_U}{2\pi} + \frac{(\Gamma_V+\Gamma_U)(5\Gamma_V+7\Gamma_U)}{24\pi^2}\right],$$

$$\frac{d\Gamma_U}{d\ln M} = \Gamma_U\left[1 - \frac{3(\Gamma_V+\Gamma_U)}{2\pi} + \frac{(\Gamma_V+\Gamma_U)(5\Gamma_V+7\Gamma_U)}{24\pi^2}\right].$$

It turns out that despite their structural similarity of these equations the fates of two types of disorders are very distinct as depicted in Fig. 16. If we include one-loop corrections only (left), there appear two critical lines each for Γ_V and Γ_U. Over the red line Γ_U starts to increase and over the blue line Γ_V does, too. However, the total gradient is overwhelmed by that of Γ_U, i.e., almost upward. This means that the antiscreening of Γ_V is much weaker than that of Γ_U. If we include two-loop corrections also that give rise to screening in both disorders (right), there appears another critical line for Γ_U while the critical line for Γ_V disappears, so Γ_V becomes irrelevant. As a result, we have two nonzero fixed points on the line of $\Gamma_V = 0$ as shown in this figure and the first figure in Fig. 3.

This observation suggests that Γ_U has dominant effects over Γ_V for the low-energy physics. Since we are interested in the renormalization of c_k, we need to consider two equations at $\Gamma_V = 0$:

$$\frac{d\Gamma_U}{d\ln M} = \Gamma_U\left[1 - a_\Gamma\Gamma_U + b_\Gamma\Gamma_U^2\right],$$
$$\frac{dc_k}{d\ln M} = c_k\left[-1 - a_c\Gamma_U + b_c\Gamma_U^2\right],$$

where the positive numerical constants are given by

$$a_\Gamma = \frac{3}{2\pi}, \quad b_\Gamma = \frac{7}{24\pi^2}, \quad a_c = \frac{1}{2\pi}, \quad b_c = \frac{1}{12\pi^2}.$$

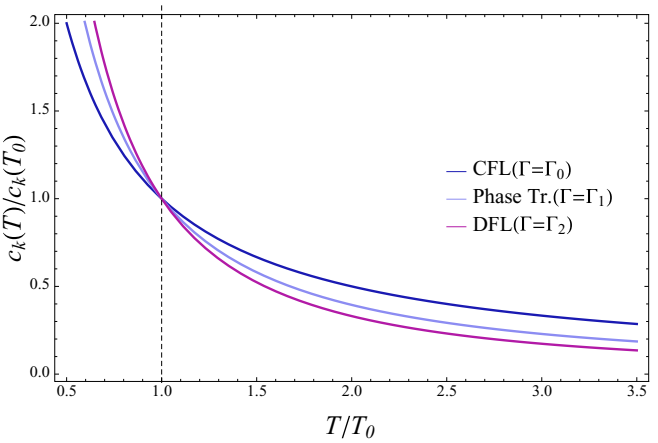

FIG. 17. Evolution of c_k with temperature (T) near each fixed point. At the clean Fermi liquid (CFL) ($\Gamma = \Gamma_0$), the exponent of c_k is $\lambda_{c,f0} = 1$ as the dimensional analysis suggests. On the other hand, at the phase transition point ($\Gamma = \Gamma_1$) and diffusive Fermi liquid (DFL) ($\Gamma = \Gamma_2$), the exponents of c_k are changed to be $\lambda_{c,f1} \simeq 1.34$ and $\lambda_{c,f2} \simeq 1.60$, respectively, due to additional contributions from nonzero values of Γ.

In the first equation for Γ_U, there are three fixed points: $\Gamma_0 = 0, \Gamma_1 = \frac{a_\Gamma - \sqrt{a_\Gamma^2 - 4b_\Gamma}}{2b_\Gamma}$, and $\Gamma_2 = \frac{a_\Gamma + \sqrt{a_\Gamma^2 - 4b_\Gamma}}{2b_\Gamma}$. Two stable fixed points of Γ_0 and Γ_2 are identified as a clean Weyl metal state and a diffusive Weyl metal phase, respectively. An unstable fixed point of Γ_1 is identified as the phase transition point from the clean Weyl metal state to the diffusive Weyl metal phase.

Let us move on the second equation for c_k. The formal solution is given by

$$c_k(T) = c_k(T_0)\exp\left[-\int_{\ln T_0}^{\ln T} d\ln M - a_c\int_{\ln T_0}^{\ln T} d\ln M\,\Gamma_U(M) + b_c\int_{\ln T_0}^{\ln T} d\ln M\,\Gamma_U^2(M)\right],$$

where T_0 is a UV cutoff. Inserting the solution of $\Gamma_U(M)$ into the above, we find that the distance between the pair of Weyl points shows a power-law divergent behavior

$$c_k(T) = c_k(T_0)\left(\frac{T_0}{T}\right)^{\lambda_{c,fn}}, \tag{E3}$$

where $\lambda_{c,fn}$ is a critical exponent around each fixed point, given by

$$\lambda_{c,f0} = 1 + a_c\Gamma_0 - b_c\Gamma_0^2 = 1,$$
$$\lambda_{c,f1} = 1 + a_c\Gamma_1 - b_c\Gamma_1^2 \simeq 1.34,$$
$$\lambda_{c,f2} = 1 + a_c\Gamma_2 - b_c\Gamma_2^2 \simeq 1.60.$$

Disorder scattering changes the temperature-dependent exponent of c_k (see Fig. 17).

[1] A. O. Gogolin, A. A. Nersesyan, and A. Tsvelik, *Bosonization and Strongly Correlated Systems* (Cambridge University Press, New York, 1998).

[2] T. Senthil, A. Vishwanath, L. Balents, S. Sachdev, and M. P. A. Fisher, Science **303**, 1490 (2004); T. Senthil, L. Balents, S. Sachdev, A. Vishwanath, and M. P. A. Fisher, Phys. Rev. B **70**, 144407 (2004).

[3] A. Tanaka and X. Hu, Phys. Rev. Lett. **95**, 036402 (2005).

[4] E. Fradkin, *Field Theories of Condensed Matter Physics* (Cambridge University Press, New York, 2013).

[5] F. Evers and A. D. Mirlin, Rev. Mod. Phys. **80**, 1355 (2008).

[6] A. M. M. Pruisken, Nucl. Phys. B **235**, 277 (1984); **240**, 30 (1984).

[7] L. Fu and C. L. Kane, Phys. Rev. Lett. **109**, 246605 (2012).

[8] For a review, see Ki-Seok Kim, Heon-Jung Kim, M. Sasaki, J.-F. Wang, and L. Li, Sci. Technol. Adv. Mater. **15**, 064401 (2014).

[9] M. E. Peskin and D. V. Schroeder, *An Introduction to Quantum Field Theory* (Addison Wesley, New York, 1995).

[10] K.-M. Kim, Y.-S. Jho, and K.-S. Kim, Phys. Rev. B **91**, 115125 (2015).

[11] F. D. M. Haldane, Phys. Rev. Lett. **93**, 206602 (2004).

[12] S. Murakami, New J. Phys. **9**, 356 (2007).

[13] A. A. Burkov and L. Balents, Phys. Rev. Lett. **107**, 127205 (2011).

[14] H. B. Nielsen and M. Ninomiya, Phys. Lett. B **130**, 389 (1983).

[15] H.-J. Kim, K.-S. Kim, J.-F. Wang, M. Sasaki, N. Satoh, A. Ohnishi, M. Kitaura, M. Yang, and L. Li, Phys. Rev. Lett. **111**, 246603 (2013).

[16] D. T. Son and B. Z. Spivak, Phys. Rev. B **88**, 104412 (2013).

[17] K.-S. Kim, H.-J. Kim, and M. Sasaki, Phys. Rev. B **89**, 195137 (2014).

[18] A. Altland, D. Bagrets, L. Fritz, A. Kamenev, and H. Schmiedt, Phys. Rev. Lett. **112**, 206602 (2014); A. Altland, D. Bagrets, and A. Kamenev, Phys. Rev. B **91**, 085429 (2015).

[19] A. Altland and D. Bagrets, Phys. Rev. B **93**, 075113 (2016).

[20] Y.-S. Jho, J.-H. Han, and K.-S. Kim, arXiv:1409.0414.

[21] Mathematically speaking, the factor 3 difference in the renormalization group equations for intravalley and intervalley scattering originates from the sign difference in the renormalization constants of $Z_{\Gamma V}$ and $Z_{\Gamma U}$ in Eq. (E1) of Appendix E. This sign difference means that the intravalley-scattering vertex is screened as expected while the intervalley-scattering vertex is antiscreened: The intervalley-scattering vertex becomes enhanced at low temperatures. As a result, the physics is governed by the intervalley scattering. Physically, this may be understood in the following way. The intervalley scattering mixes the chirality while the intravalley scattering does not. Recall that the chirality is essential for the chiral anomaly. The chiral gauge field is identified with the gradient of the θ coefficient of the topological-in-origin θ term. In this respect it is natural to expect that the intervalley scattering would play a predominant role in the renormalization for the chiral gauge field, i.e., the distance between a pair of Weyl points.

[22] A. Altland and B. Simons, *Condensed Matter Field Theory* (Cambridge University Press, New York, 2010).

[23] Ki-Seok Kim, Phys. Rev. B **90**, 121108(R) (2014).

[24] D. Xiao, M.-C. Chang, and Q. Niu, Rev. Mod. Phys. **82**, 1959 (2010).

[25] N. Nagaosa, J. Sinova, S. Onoda, A. H. MacDonald, and N. P. Ong, Rev. Mod. Phys. **82**, 1539 (2010).

[26] P. Goswami and Sumanta Tewari, Phys. Rev. B **88**, 245107 (2013).

[27] A. A. Zyuzin and A. A. Burkov, Phys. Rev. B **86**, 115133 (2012).

[28] Y. Chen, D. L. Bergman, and A. A. Burkov, Phys. Rev. B **88**, 125110 (2013).

[29] K. Fukushima, D. E. Kharzeev, and H. J. Warringa, Phys. Rev. D **78**, 074033 (2008).

[30] D. T. Son and N. Yamamoto, Phys. Rev. Lett. **109**, 181602 (2012).

[31] M. A. Stephanov and Y. Yin, Phys. Rev. Lett. **109**, 162001 (2012).

[32] G. Basar, D. E. Kharzeev, and H.-U. Yee, Phys. Rev. B **89**, 035142 (2014).

[33] K. Landsteiner, E. Megias, and F. Pena-Benitez, Phys. Rev. Lett. **107**, 021601 (2011).

[34] Y. Chen, Si Wu, and A. A. Burkov, Phys. Rev. B **88**, 125105 (2013).

[35] D. T. Son and N. Yamamoto, Phys. Rev. D **87**, 085016 (2013).

[36] C. Manuel and Juan M. Torres-Rincon, Phys. Rev. D **90**, 076007 (2014).

[37] J.-Y. Chen, D. T. Son, M. A. Stephanov, Ho-Ung Yee, and Yi Yin, Phys. Rev. Lett. **113**, 182302 (2014).

[38] I. Zahed, Phys. Rev. Lett. **109**, 091603 (2012).

[39] G. Basar, D. E. Kharzeev, and I. Zahed, Phys. Rev. Lett. **111**, 161601 (2013).

[40] C. Duval and P. A. Horvathy, Phys. Rev. D **91**, 045013 (2015).

[41] M. Stone, V. Dwivedi, and T. Zhou, Phys. Rev. D **91**, 025004 (2015).

[42] Y.-S. Jho and K.-S. Kim, Phys. Rev. B **87**, 205133 (2013).

[43] D. Shin, Y.-W. Park, M. Sasaki, H.-J. Kim, Y.-H. Jeong, K.-S. Kim, and J. Kim (unpublished).

[44] R. D. Peccei and H. R. Quinn, Phys. Rev. Lett. **38**, 1440 (1977); M. ElAfioni, M. Gomes, and R. Koberle, Phys. Rev. D **19**, 1791 (1979).

[45] W. J. den Dunnen, Master's thesis, Vrije Universiteit, Amsterdam, 2008 (unpublished).

[46] D. Vollhardt and P. Wölfle, Phys. Rev. B **22**, 4666 (1980); in *Electronic Phase Transitions*, edited by W. Hanke, and Yu. V. Kopaev (North-Holland, Amsterdam, 1992).